

## ARTICLE

## Seafloor reflector imaging in 2D seismic data through muting of out-of-plane signals in the Ulleung Basin, East Sea

Ganghoon Lee<sup>1</sup>, Changyoon Lee<sup>1</sup>, Junseok Kwon<sup>1</sup>, and Snons Cheong<sup>2\*</sup><sup>1</sup>Resource Exploration & Development Research Division, Korea Institute of Geoscience and Mineral Resources, Daejeon, Yuseong-gu, Republic of Korea<sup>2</sup>Geo-Environment Research Division, Korea Institute of Geoscience and Mineral Resources, Daejeon, Yuseong-gu, Republic of Korea

## Abstract

Irregular topography can generate out-of-plane signals (OPS) on seismic sections, interfering with the imaging of the true seafloor directly beneath the survey line. While acquiring three-dimensional data or using specialized sensors can mitigate this, these options are often costly or unavailable, especially for legacy surveys. To efficiently remove OPS from two-dimensional (2D) data, this study investigates the validity of using a neural network (NN) for picking and muting. First, we demonstrate the limitation of conventional frequency–wavenumber domain directional filtering due to the kinematic similarity between OPS and true seafloor reflections. Then, we present a workflow that employs a cascade–correlation learning algorithm to identify and mute OPS arrivals before the first break. Unlike data-intensive deep learning techniques that require large training datasets, this lightweight NN is trained on user-picked examples of true seafloor reflections, enabling it to distinguish OPS events arriving from outside the vertical survey plane. Application of this technique to a 2D line acquired near irregular seafloor topography in the Ulleung Basin demonstrates the true seafloor reflector and the removal of false offline signals. Qualitative and quantitative validation against an independent external bathymetric reference both showed a reduction in travel time error compared to the raw data, confirming the effectiveness of the picking results. The results highlight that a cascade–correlation NN-based picking and muting can efficiently suppress OPS in cases of irregular topography on 2D seismic data.

**\*Corresponding author:**  
Snons Cheong  
(snons@kigam.re.kr)

**Citation:** Lee G, Lee C, Kwon J, Cheong S. Seafloor reflector imaging in 2D seismic data through muting of out-of-plane signals in the Ulleung Basin, East Sea. *J Seismic Explor.* 2026;35(2):025470116. doi: 10.36922/JSE025470116

**Received:** November 21, 2025

**Revised:** February 4, 2026

**Accepted:** February 27, 2026

**Published online:** April 30, 2026

**Copyright:** © 2026 Author(s). This is an Open-Access article distributed under the terms of the Creative Commons Attribution License, permitting distribution, and reproduction in any medium, provided the original work is properly cited.

**Publisher's Note:** AccScience Publishing remains neutral with regard to jurisdictional claims in published maps and institutional affiliations.

**Keywords:** Out-of-plane signal; Neural network picking and muting; True seafloor; Ulleung Basin

## 1. Introduction

Marine seismic surveys are common tools for exploring the Earth's subsurface beneath oceans and seas, with two-dimensional (2D) profiles, in particular, providing valuable insights into geological structures and stratigraphy.<sup>1</sup> These surveys typically involve a vessel towing an energy source and an array of receivers (streamer), allowing efficient acquisition that yields extensive coverage and high-fold data compared to onshore surveys. Despite these operational advantages, seismic data acquired in the marine

setting are often affected by various types of noise from the environment and the acquisition geometry itself, which can interfere with the interpretation of subsurface targets. Standard seismic data processing aims to enhance the desired signals and attenuate noise, producing a clearer image of the subsurface.<sup>2</sup> However, one type of coherent noise, often encountered when surveying areas characterized by irregular seafloor morphology, poses a particular challenge. This challenge stems from energy reflecting off features that are lateral to the intended 2D survey line. These signals, known as out-of-plane signals (OPS),<sup>3</sup> are sometimes also referred to as sideswipe noise.

Out-of-plane signals originate from irregular seafloor topography or subsurface structures outside the vertical plane of the seismic profile but arrive at the receivers, contaminating the seismic section.<sup>4</sup> As this out-of-plane energy is imaged within the 2D section, it generates false reflectors at apparent depths that may be either deeper or shallower than the true reflection point. A single continuous reflector can then appear as a challenging pattern of discontinuous reflections on the final image.<sup>3,5</sup> These shifted events appear as coherent signals on seismic records but do not correspond to true subsurface structures directly under the line, often leading to misinterpretation if not recognized.<sup>6</sup> As Tucker<sup>7</sup> noted, such out-of-plane energy will almost always be present when 2D lines are shot at orientations other than perpendicular to dip or structural trends. In crooked-line surveys, this problem is particularly severe. The scattered midpoint geometry, combined with cross-profile-dipping reflectors, introduces significant travel time distortions known as cross-dip moveout (CDMO), which degrades the quality of standard common midpoint stacking if not properly addressed.<sup>8</sup> From a geometrical perspective, crooked-line surveys can be regarded as a limited swath three-dimensional (3D) investigation, and in principle, 3D prestack migration provides an appropriate means to image reflectivity in the surrounding volume.<sup>9</sup> However, applying 3D processing to crooked-line data is rarely practical, and interpreters are usually constrained to legacy 2D workflows. Accurate imaging of the true seafloor is important, especially when utilizing legacy 2D data to plan new infrastructure such as submarine cables or structure construction, or to site ocean-bottom instruments. In these engineering or site-survey applications, removing OPS becomes crucial for reliable interpretation. Despite its importance, the specific problem of OPS removal has received relatively less attention.

The most direct solution is acquiring full 3D seismic data, which resolves the true 3D geometry and largely eliminates ghost or sideswipe reflections from offline

features, except perhaps near the survey edges.<sup>10-13</sup> Consequently, data-processing approaches are typically employed, but these approaches also suffer from significant limitations. However, 3D surveys are more expensive and may not be feasible for regional studies or when working with existing legacy 2D datasets. In 2D data processing, interpreters sometimes resort to manually muting suspected OPS events or attempt to design survey layouts that avoid proximity to strong lateral reflectors. Other processing approaches include specialized techniques such as frequency-wavenumber (F-K) directional filtering or polarization filtering (when multi-component data are available) to attenuate energy that does not propagate in the inline direction.<sup>14</sup> For multi-streamer or swath-acquisition geometries, this out-of-plane energy can sometimes be identified by its characteristic arrival-time differences across the receivers, often producing a distinctive “sawtooth pattern” when data are sorted in the crossline direction. This property enables targeted suppression through array processing techniques such as null steering.<sup>15</sup> More advanced approaches employ iterative processing workflows that correct for CDMO and then recalculate velocities and dip moveout (DMO), though these can produce artifacts such as duplicated reflection events if not applied carefully.<sup>16</sup> To mitigate this, generalized CDMO (GCDMO) methods have been introduced, designed to operate on curved acquisition geometries, thereby reducing such artifacts.<sup>17</sup> 3D effects present such a challenge that even advanced operators like azimuth moveout inherently contain out-of-plane, skewed-saddle characteristics.<sup>18</sup> To address this issue, velocity-independent, slope-based time-domain DMO techniques were developed that use local event slopes to circumvent the iterative cycle between velocity analysis and DMO correction.<sup>19</sup> However, these approaches can be challenging to apply in practice to field survey data. OPS events often exhibit moveouts and wavelet characteristics similar to those of genuine reflections from beneath the survey line, making them difficult to separate using standard filtering techniques. Simple filtering also carries the risk of removing valid dipping events or diffractions that are part of the true subsurface image.

Distinguishing OPS from the true seafloor reflection based solely on visual inspection or conventional filtering is often difficult. These challenges highlight the need for a more targeted approach capable of accurately identifying the true seafloor reflection amidst the interfering OPS arrivals, a task for which conventional methods often prove inadequate. Furthermore, advanced techniques such as polarization filtering and GCDMO have limited applicability to legacy 2D datasets. Polarization filtering requires multi-component data, which is unavailable

in standard hydrophone streamer surveys. Similarly, deterministic GCDMO requires accurate cross-dip information, which is ill-posed to resolve using a single 2D line without 3D spatial sampling. These constraints highlight the need for a method that relies on morphological pattern recognition within the available scalar 2D data.

A further complication is that OPS can arise in different aspects of the seismic section. Depending on the geometry of the interfering structures, OPS may occur either before or after the true seafloor reflection. This overlap makes it particularly challenging in engineering and site-survey applications, where precise seafloor imaging is essential for placing infrastructure such as submarine cables or ocean-bottom instruments. By contrast, post-arrival OPS originates from deeper or more distant structures, where the signals mix with other lateral reflections and diffractions. These situations are more difficult to address with 2D methods and are often better suited to 3D imaging or advanced machine learning approaches that can use larger datasets. In this study, we concentrate on the pre-arrival case, which is both widespread and critical for practical applications because it directly overlaps with the water-bottom event. Our motivation arises from the fact that the first break picking can be used as a mute parameter to remove the OPS. This study uses and validates a semi-automated workflow that employs a lightweight, supervised neural network (NN) to accurately pick the true seafloor reflection, thereby enabling the muting of pre-arrival OPS. We apply this method to a 2D marine seismic line from the Ulleung Basin, in the East Sea, an area where irregular seafloor topography generates significant out-of-plane energy. This paper demonstrates that a targeted, picking-based workflow can effectively suppress OPS, improving the continuity and fidelity of the seafloor reflector in the final seismic image and offering a practical solution for enhancing the quality of legacy 2D seismic data.

## 2. Data and methodology

### 2.1. The study area and seismic data

The study area is located on the continental shelf and slope of the Ulleung Basin in the East Sea (Figure 1A).<sup>20</sup> The basin features water depths that generally increase from west to northeast. Notable seafloor topographic features create sudden changes in bathymetry (Figure 1B). To investigate structural and sedimentological variations, a 2D seismic survey was conducted in 2017. The seismic data were collected along an approximately 170 km line trending Northeast–Southwest (NE–SW) (shooting direction 225°). Key acquisition parameters are listed in Table 1. Near the northeastern part, adjacent to the start of the line, significant out-of-plane scattering originating

from the irregular seafloor topography lateral to the survey track was observed (dashed box in Figure 1B and 1D). The complex 3D bathymetry of the survey area is further illustrated in the 3D views (Figure 1C). Figure 1D presents a zoomed 3D view of the dashed-box region alongside a brute-stack section, clearly showing false reflectors caused by the OPS.

These signals arrive earlier than the true seafloor reflection directly beneath the vessel. This occurs because the wavepath from the shallower, offline topographic features can be shorter than the path to the deeper seafloor directly below the line, even though the horizontal distance is greater. The workflow is specifically tailored for the common case where OPS from shallower, offline topography arrives before the true seafloor reflection. This pre-arrival OPS case is particularly challenging because it can lead to seafloor positioning errors for engineering applications. Conceptually, the two-way travel time for the true reflection ( $t_{true}$ ) versus the OPS ( $t_{OPS}$ ) can be compared:

$$t_{true} = \frac{2D_{vertical}}{V_{water}} \quad (1)$$

$$t_{OPS} = \frac{Slant\ path\ length}{V_{water}} \quad (2)$$

where,  $D_{vertical}$  is the water depth directly beneath the survey line, and  $V_{water}$  is the velocity of a seismic wave in water. Due to the geometry illustrated in Figure 2, it is often the case that  $t_{OPS} < t_{true}$  when significant lateral topography exists at shallower depths than the seafloor below the vessel. Figure 2 provides a conceptual illustration showing how reflections from lateral seafloor topography can generate OPS that interferes with the desired reflection from the seafloor directly beneath the survey vessel in a 2D marine survey.

The entire brute-stacked section images the NE–SW trending Ulleung Basin, revealing shallow seafloor reflections at the ends of the line and a central slope region underlain by features interpreted as debris-flow and turbidite deposits (Figure 3A).<sup>21,22</sup> Figure 3B presents seven representative shot gathers sampled along the line.

An enlarged view of the target zone shows both relatively flat seafloor areas and the transition to the slope region (Figure 4A). Seismic trace headers usually contain recorded water bottom times. Figure 4B shows the result of applying a mute based on the water bottom time in the header information. However, this header-derived time is unreliable as it can be influenced by both the true seafloor reflection and strong OPS arrivals, as well as potential

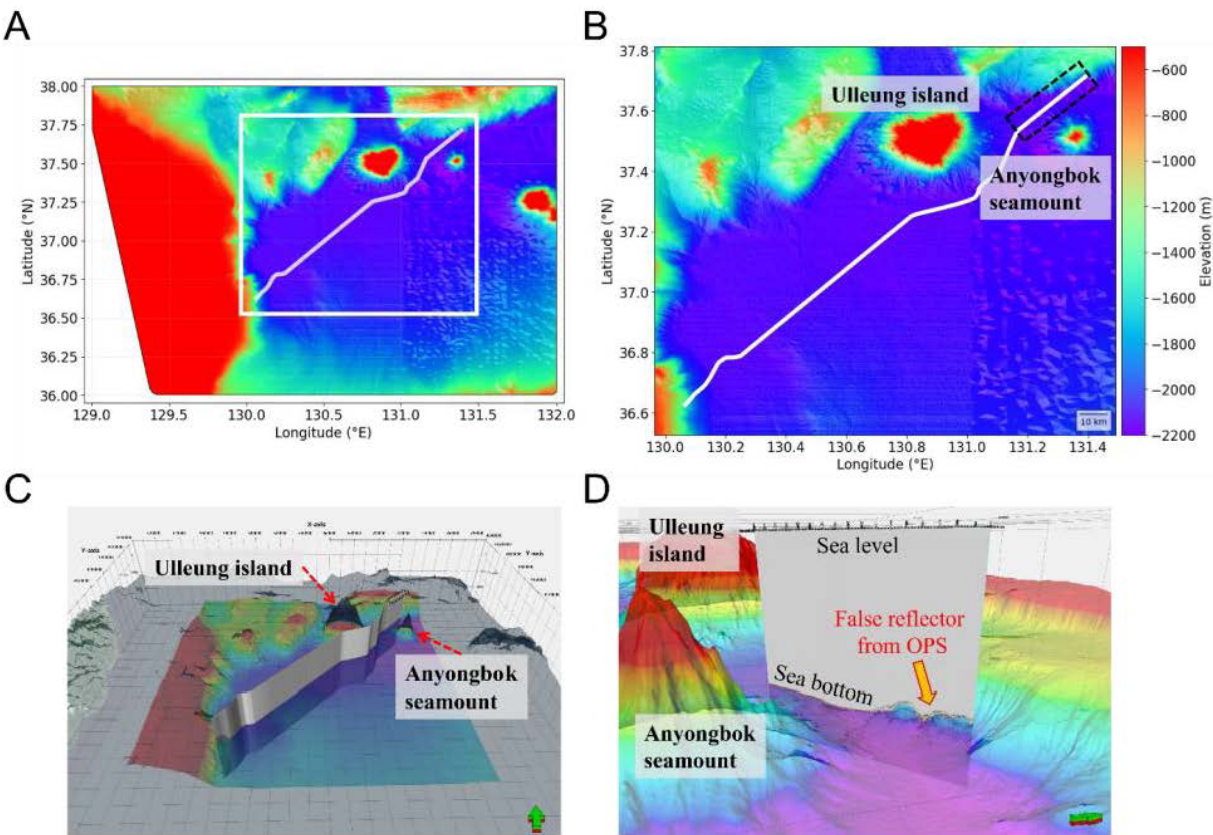


**Figure 1.** Overview of the survey area and geometry in the Ulleung Basin, East Sea. (A) Bathymetric map of the study region, with color shading indicating elevation above and depth below sea level; the white rectangle outlines the area enlarged in panel (B). (B) Zoom-in of the boxed region in (A) showing the vessel's survey track as a white line denoting the survey line; the dashed box highlights an area with significant out-of-plane signal (OPS); the scale bar in the lower right represents 10 km. (C) Three-dimensional perspective view of the survey area bathymetry. (D) Zoom-in three-dimensional perspective view of the dashed box region in (B), illustrating the seafloor topography causing OPS.

**Table 1.** Key acquisition parameters for the two-dimensional marine seismic survey in the Ulleung Basin

Parameter	Value
Number of channels	456
Group interval (m)	12.5
Sampling interval (ms)	1
Recording length (s)	7.0
Air-gun volume (in <sup>3</sup> )	2,289
Shot interval (m)	25.0
Shooting direction (degree)	225



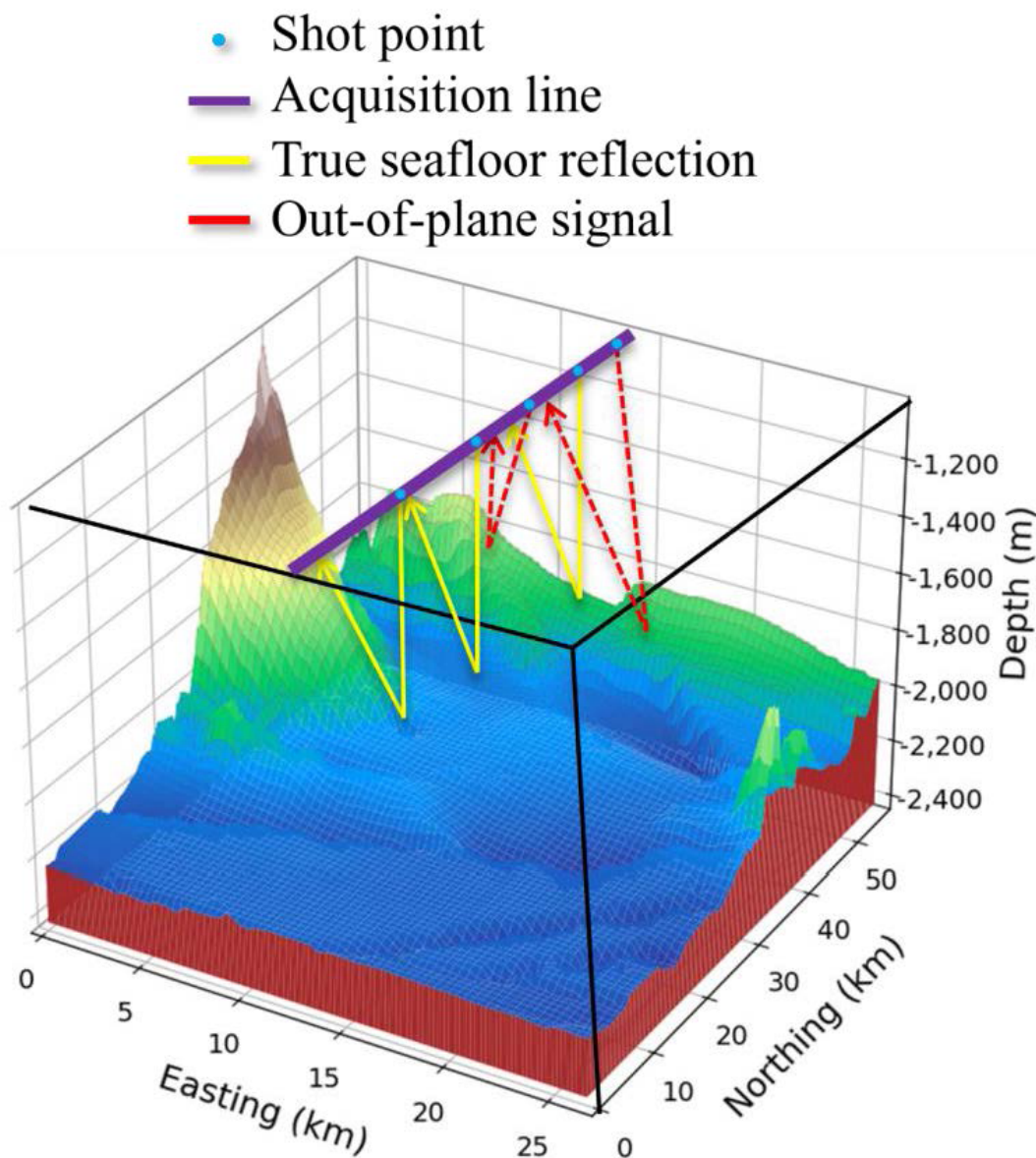
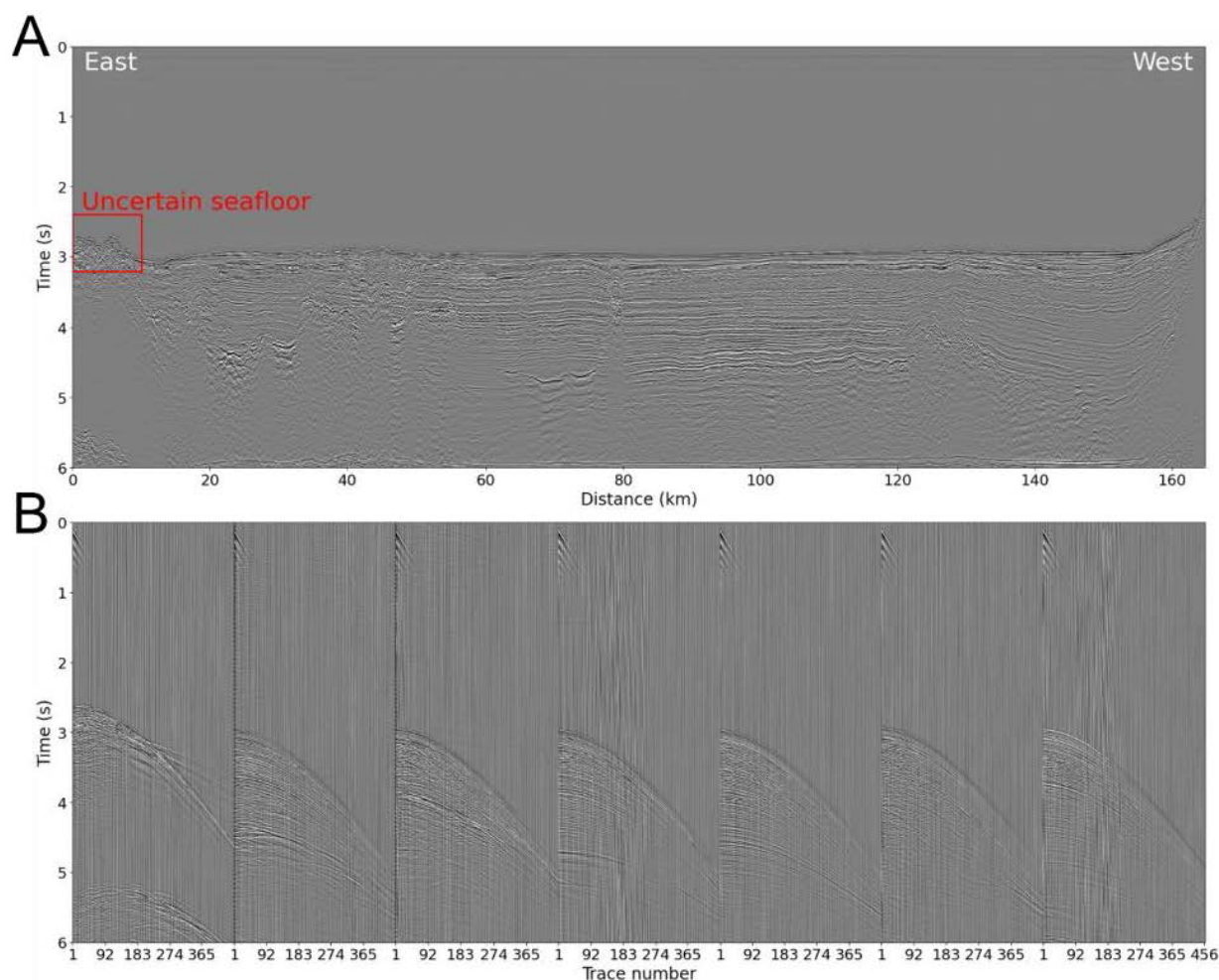


**Figure 2.** Conceptual illustration (pseudo-three-dimensional perspective) showing the generation of out-of-plane signal in a two-dimensional marine survey due to complex seafloor topography. The seismic source emits energy that reflects from the true seafloor directly beneath the vessel (solid yellow raypath, “true seafloor reflection”) and also reflects off lateral topographic features outside the survey line (dashed red raypaths, “out-of-plane signal”) arriving at the receiver and potentially interfering with the true reflection.

noise from instrument errors or weather conditions (dashed green arrows). Consequently, the mute based solely on the water bottom time in the header does not effectively remove the OPS and clarify the true seafloor. This result indicates that a simple, header-based approach is insufficient for accurate OPS removal in this dataset, motivating the evaluation of more advanced processing techniques.

## 2.2. Limitations of the conventional method: frequency-wavenumber filtering

As a baseline for comparison, we first assess the effectiveness of F-K directional filtering, a conventional method for attenuating coherent noise. We applied the filter independently to the same three domains used in our study, namely common shot gathers, common receiver gathers, and common depth point (CDP)-offset gathers.



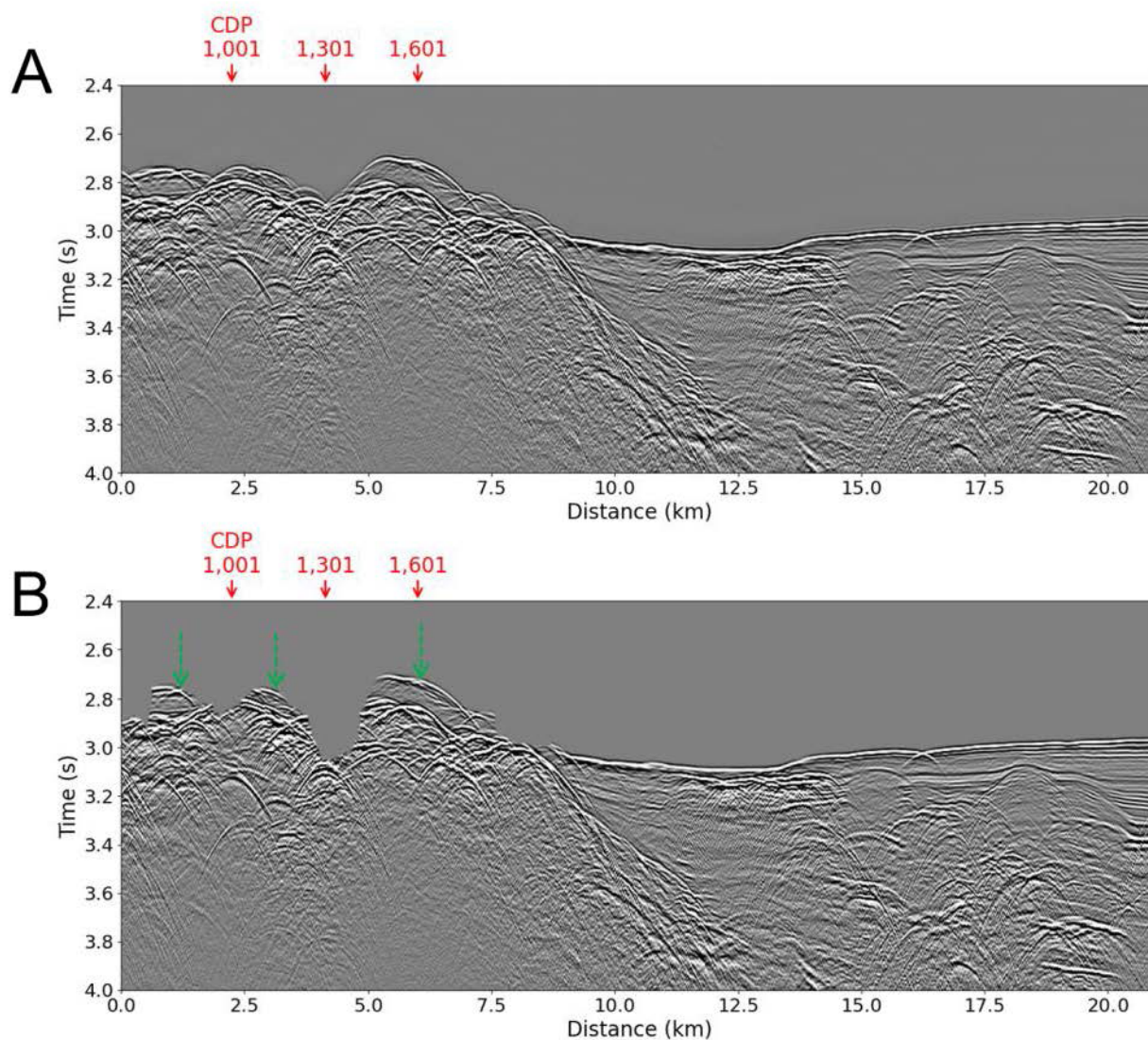
**Figure 3.** (A) Brute-stacked seismic section of the full line, with two-way travel time on the vertical axis and inline distance on the horizontal; the red box highlights the zone where the seafloor reflector is masked by out-of-plane signal. (B) Seven representative shot gathers were extracted at equal intervals along the line.

Figure 5 presents the F–K spectra before and after filtering for a representative gather from each domain.

The F–K spectra demonstrate that OPS energy exhibits an apparent moveout (dip) nearly identical to that of the true seafloor reflection. Consequently, their energy overlaps in the F–K domain, which prevents effective dip-selective filtering. Even with aggressive filtering applied, OPS events remained largely within the sections. The stacked sections in Figure 6 further confirm that OPS energy was only weakly suppressed and remained clearly visible after filtering. The failure of this conventional dip-based approach underscores the need for an alternative method capable of distinguishing OPS from true seafloor reflections using a broader combination of waveform attributes beyond just dip.

### 2.3. Neural network-based seafloor picking and muting

To overcome the limitations of conventional filtering, we use a technique centered on accurately picking the true seafloor reflection event and muting the preceding OPS arrivals. Our approach employs a supervised NN to learn the characteristics of the desired seafloor event from user-provided examples. Early studies demonstrated that NNs could automate seismic interpretation tasks, such as first-break picking by learning directly from data.<sup>23,24</sup> While modern deep learning techniques such as convolutional neural networks have shown success, they often require large labeled datasets,<sup>25,26</sup> which are rarely available for legacy 2D data with specific noise problems, such as OPS. Recent advances in machine learning have shown great



**Figure 4.** Enlarged view of the seafloor zone affected by out-of-plane signal (OPS) (0–21 km inline, 2.4–4.0 s two-way time), illustrating the OPS event and the result of header-based muting. (A) The brute-stacked section shows a coherent OPS event appearing near the seafloor between ~2.8 s and 3.2 s; solid red arrows mark common depth point (CDP) locations 1,001, 1,301, and 1,601. (B) The same interval after applying a mute based on the water bottom time in the header information. Note the persistence of residual OPS where the header mute does not accurately follow the true seafloor (dashed green arrow).

success in seismic processing, including robust automated picking across various environments<sup>27,28</sup> and sophisticated coherent noise attenuation using deep learning.<sup>29,30</sup> However, many of these deep learning denoisers<sup>31</sup> require large, high-quality labeled datasets, which are often unavailable for legacy 2D data that suffer from specific issues such as OPS. This constraint motivates the use of a more data-efficient strategy. Therefore, for this task, we selected the cascade-correlation architecture, a lightweight NN approach known for its ability to learn effectively from a small number of user-provided examples.<sup>32,33</sup> This makes

it a practical choice for our specific goal of suppressing OPS in legacy data without requiring extensive pre-labeled datasets. The process involves defining a time window, manually picking the true seafloor event on a few traces, training the NN on these picks, and then applying the trained network to pick the event automatically on all traces within the target zone (Figure 7). The neural network inputs consist of seismic trace amplitudes extracted from a user-defined time window centered on the manually picked event. This window, or “gate,” allows the network to capture the local waveform shape and moveout characteristics of



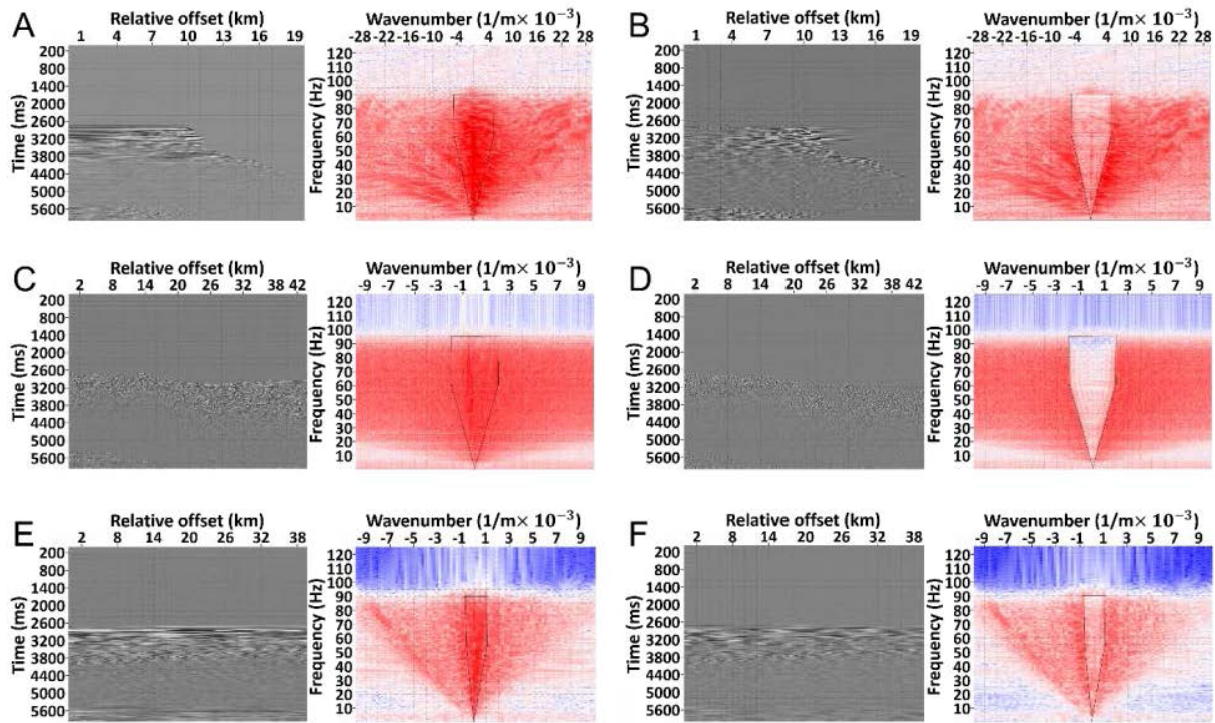


**Figure 5.** Representative gathers and their F–K spectra before and after F–K directional filtering. (A, B) Common shot gather. (C, D) Common receiver gathers. (E, F) Common depth point–offset gather. Note the spectral overlap between the seafloor reflection and the out-of-plane signal energy, which limits the effectiveness of dip-selective filtering.

the true seafloor reflection. For this study, the gate was set to encompass approximately two periods of the dominant frequency around the first break. The network minimizes the error between the manual pick time and its predicted arrival time by adjusting the weights of the added hidden units. The specific training parameters used are detailed in Table 2. Arrival time was predicted by fitting a line to several previous picks using the slope of the top gates. Thus, the window in which the network considers a pick can be restricted to a small range about the predicted arrival time of the first break. Once the NN pick determines the arrival time of the true seafloor reflection, this horizon information is converted into a mute table, which is then used to apply a top mute, removing energy arriving before the picked time (i.e., the OPS). This workflow is designed to generate an accurate time horizon for the true seafloor that can be used for muting or other interpretation purposes.

#### 2.4. The cascade–correlation architecture

To discriminate OPS from true reflections, we employed the NN picking tool available in Landmark’s SeisSpace processing software. This tool utilizes a supervised artificial neural network based on the cascade–correlation

architecture developed by Fahlman and Lebiere.<sup>32</sup> Unlike standard backpropagation networks, which adjust weights within a fixed architecture, cascade–correlation incrementally builds the network structure during training. It starts with a minimal network (inputs connected directly to outputs) and then iteratively adds new hidden units one by one. Crucially, once a hidden unit is added, its input weights are frozen. Only the weights for the new unit are trained, followed by retraining only the output layer weights. A new hidden unit  $h_j$  receives connections from all input units  $x_i$  and all previously installed hidden units  $h_k$  (where  $k < j$ ). Its output  $y_j$  is calculated as

$$y_j = \sigma \left( \sum_i w_{ji} x_i + \sum_{k < j} w_{jk} y_k \right) \quad (3)$$

where  $w$  are the input weights and  $\sigma$  is an activation function (e.g., sigmoid). Each new hidden unit is trained to maximize the correlation between its output and the residual error signal that the existing network has not yet learned. Specifically, the algorithm attempts to maximize a measure  $S$ , the magnitude of the covariance between the candidate unit’s output,  $V$ , and the residual output error,

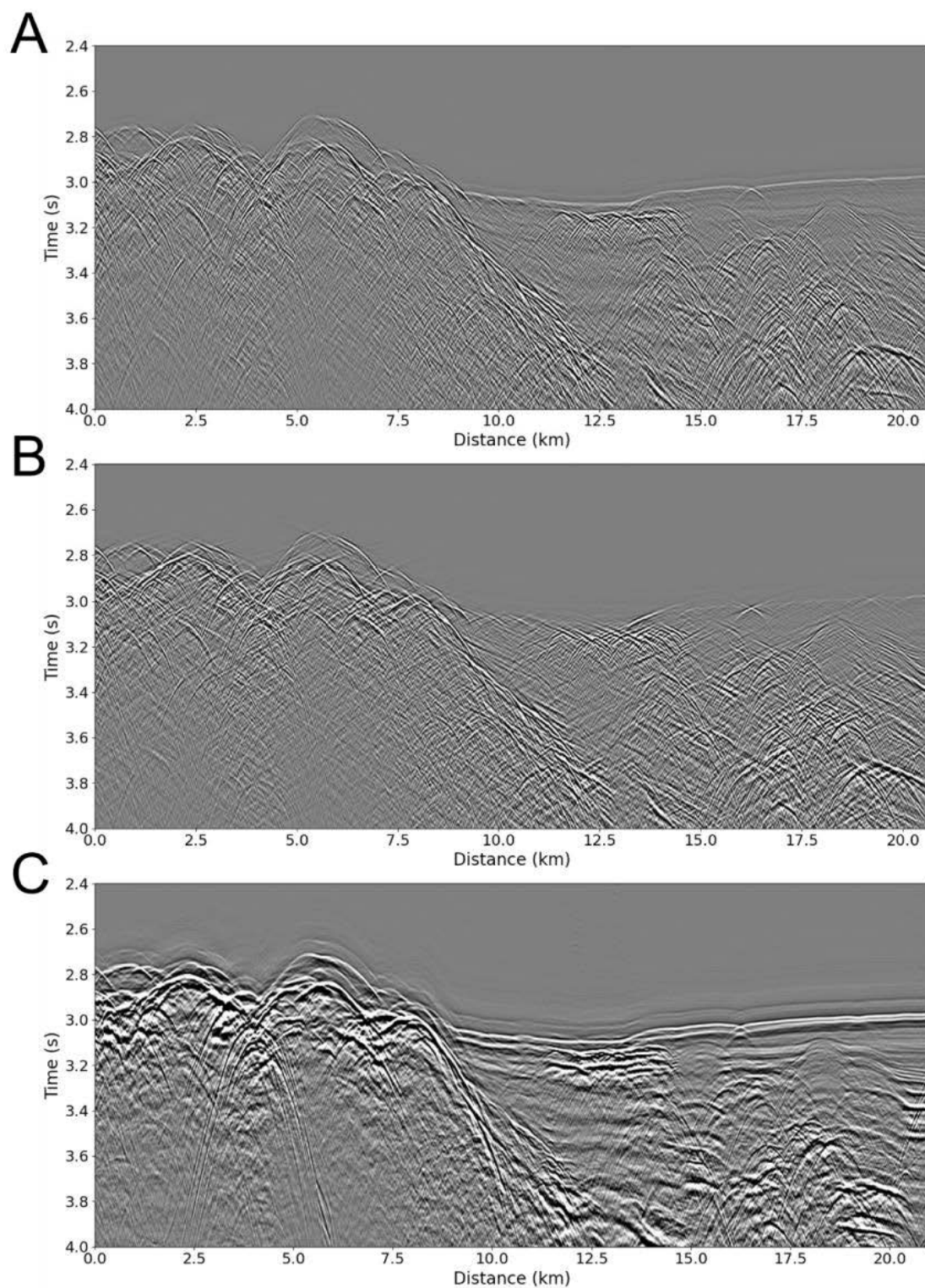


**Figure 6.** Stacked sections after F–K directional filtering were applied in the (A) common shot, (B) common receiver, and (C) common depth point-offset domains. Residual out-of-plane signal remains visible near the seafloor in all cases.



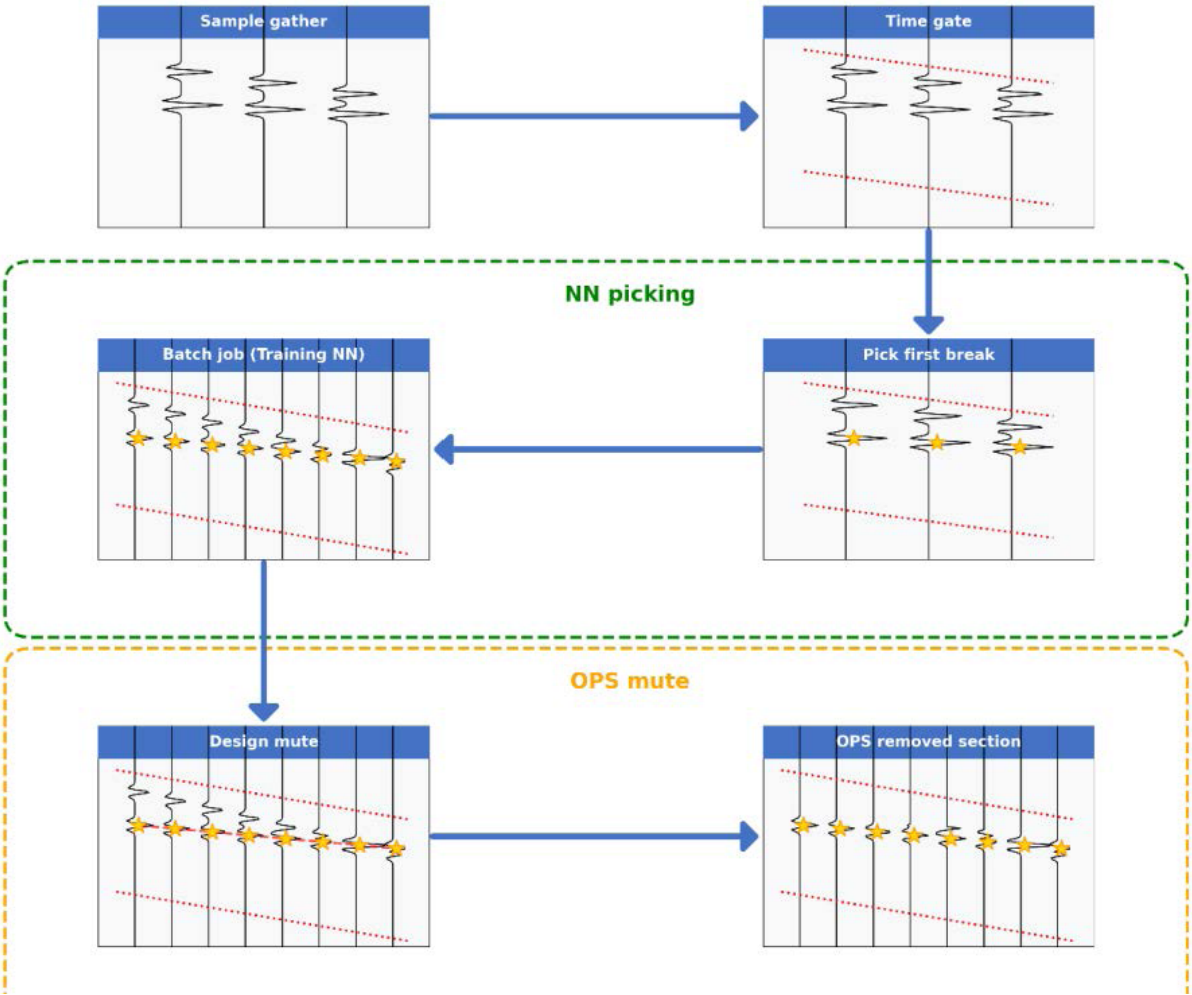


Figure 7. Processing flow to determine the mute table from the neural network (NN) pick for out-of-plane signal (OPS) removal

Table 2. Parameters in neural network for first-break (FB) picking in seismic data processing

Parameter	Value/description
Number of traces in the median line fit	6
Maximum trace-to-trace static (ms)	20.0
Starting offset to determine FB pick slope (m)	150.0
Time gate file/database name	Filepath & name

$E_o$ :

$$S = \sum_o \left| \sum_p (V_p - \bar{V})(E_{p,o} - \bar{E}_o) \right| \quad (4)$$

where the sum is over output units  $o$  and input patterns  $p$ , and  $\bar{V}$  and  $\bar{E}_o$  represent average values.

This incremental learning strategy, focusing on new units on the remaining error, allows the network to adapt its complexity to the specific problem. This approach was chosen for its efficiency and demonstrated ability to train effectively on relatively few user-provided samples. A schematic illustration of this architecture is shown in Figure 8.

### 2.5. Training process and feature recognition

The training process is an iterative, gather-by-gather workflow. First, an interpreter manually picks the entire seafloor reflection horizon on a single representative gather, which serves as the label data. The network is trained using this single, complete example and then immediately evaluated by having it predict the horizon on the very same gather. If the prediction does not closely match the manual pick, the training process is repeated to refine its parameters. This iterative training-and-evaluation loop continues until the network can accurately reproduce the manual horizon for that gather. Once the NN picking is complete, the determined travel times are saved to the seismic database and transferred to the trace headers as the seafloor arrival time. This horizon information is then directly mapped to the mute parameter header to define the top-mute function. No additional tapering or smoothing was applied during this transfer, preserving the exact pick times determined by the network.

This process is illustrated in Figure 9. The entire iterative cycle is then performed on approximately 20 different representative gathers, chosen to encompass variations in water depth and OPS intensity, to build a robust final network. The key configuration parameters of the network training are summarized in Table 3.

The primary physical features that the NN is designed to differentiate can be grouped into several categories. Residual moveout after normal moveout (NMO) correction provides the most important feature, since the true in-plane seafloor reflection becomes relatively flat while OPS retains curvature. Additionally, lateral continuity and coherence help the network identify the true seafloor, which generally exhibits greater spatial continuity than OPS events that are more discontinuous. Finally, waveform and peak travel time provide an additional constraint, as the implementation was designed to track the travel time

of the reflection's peak amplitude, linking this with the other physical properties of the true seafloor. As shown in Figure 9, the network progressively refines its ability to combine these indicators, aligning its predictions more closely with the interpreter-defined horizon through repeated adjustment.

### 2.6. Application in different gathering domains

The entire workflow was executed in three different gather domains to evaluate which domain yielded the best performance for OPS removal, including common shot gathers (conventional shot records in streamer surveys), common receiver gathers (grouping traces by receiver channel across all shots), and CDP-offset gathers (conventional common midpoint gathers). A separate and independent training process was carried out for each data domain. For the common shot gathers, a distinct network was trained using manual picks from that domain. The same procedure was then repeated for the common receiver and CDP-offset gathers, ensuring that each domain produced a network specifically optimized for its own data representation. Applying NMO correction to common shot gathers can help flatten the primary seafloor reflection, which may facilitate NN picking and subsequent OPS muting in this domain. Conversely, common receiver gathers typically exhibit less severe moveout for the seafloor event, often eliminating the need for NMO correction before picking, which simplifies the process and avoids potential NMO stretch artifacts. We evaluated the effectiveness of NN picking in each domain.

The network learns to distinguish the seafloor event from the OPS based on characteristics learned from the training examples, such as amplitude, frequency content, waveform shape, and continuity across traces. For instance, the OPS might have different amplitude decay or moveout characteristics compared to the true seafloor reflection originating from directly beneath the line. Because the network is trained locally on the specific survey data, it adapts to the particular noise and signal characteristics present. A key aspect of this technique is that it does not require a large labeled dataset or extensive training time like many modern deep learning approaches. The NN essentially acts as an intelligent tool to propagate the interpreter's identification of the target event across the dataset based on learned patterns.

## 3. Results

### 3.1. Application of neural network picking to seismic gathers

We applied the NN picking workflow in the three gather domains (common shot, common receiver, and CDP-

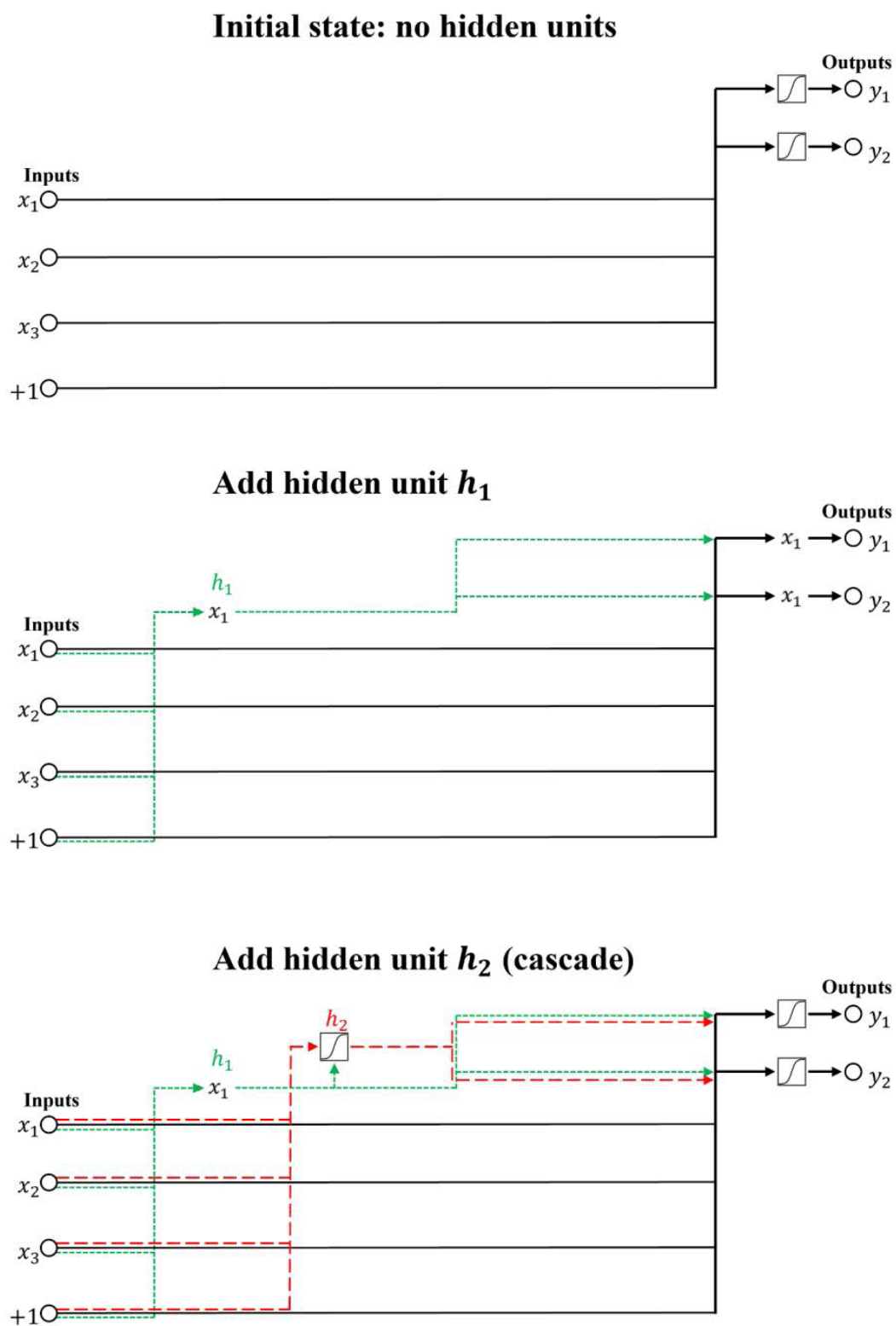


**Figure 8.** Schematic diagram of the cascade-correlation neural network architecture (adapted from Fahlman and Lebiere<sup>32</sup>). The network incrementally adds hidden units ( $h_1, h_2$ , etc.), which receive input from all previous input and hidden units. Once a unit is added, its input weights are frozen.

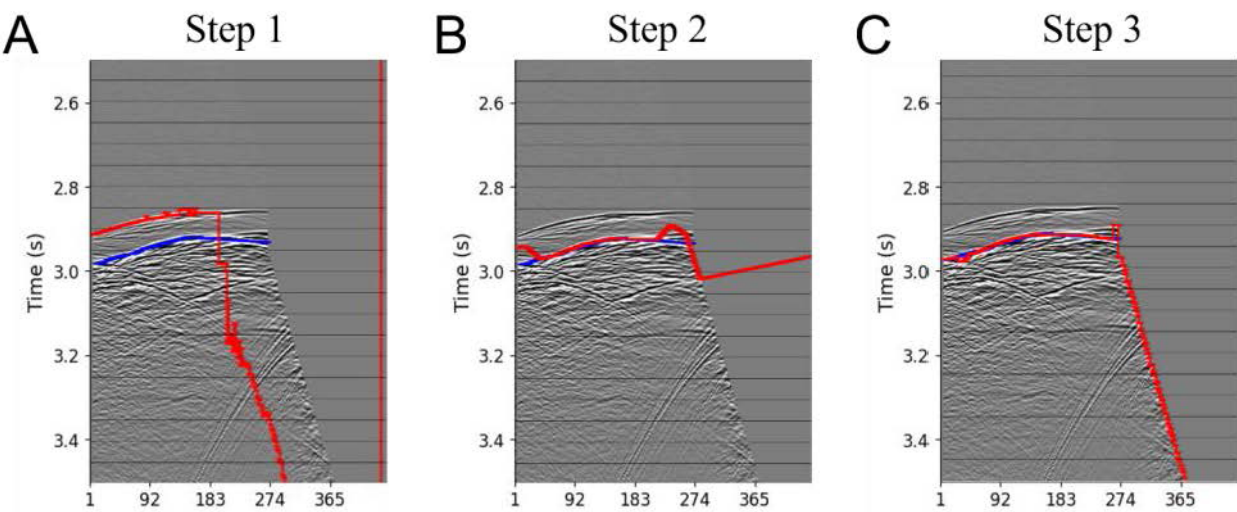


**Figure 9.** An iterative training process for the neural network on a representative dataset. The blue line is the manual pick (training label), and the red line is the neural network prediction. (A) After the first pass, the prediction is inaccurate. (B) After the second pass, the prediction improves. (C) After the third pass, the prediction converges with the manual pick.

**Table 3.** Summary of key parameters for the neural network training

Parameter	Value/description
Neural network algorithm	Cascade–correlation
Software implementation	Landmark SeisSpace (Neural Network First Break Picker module)
Training strategy	Iterative, gather-by-gather refinement
Number of training gathers	Approximately 20 representative gathers
Labeling method	Manual picking of the complete seafloor horizon on each training gather
Target feature	Peak-amplitude travel time of the seafloor reflection and the manual pick
Stopping criterion	Visual confirmation of convergence between the network’s prediction
Final application	The fully trained network is applied in batch mode to the entire dataset

offset) to assess the performance of OPS removal in each case. Figures 10, 11, and 12 illustrate representative gathers for each domain, showing the data before muting, the determined NN pick, and the gathers after muting for each domain, respectively. The gathers shown are extracted from locations near CDPs 1,001, 1,301, and 1,601, which fall within the zone affected by OPS (indicated by solid arrows in Figure 4A).

For the common shot gathers, Figure 10A displays sample NMO-corrected common shot gathers. The NMO correction adjusts the travel times based on the source-receiver offset ( $x$ ) according to the hyperbolic travel time equation:

$$t(x)^2 = t(0)^2 + \frac{x^2}{V_{NMO}^2} \quad (5)$$

where,  $t(x)$  is the two-way reflection time at offset  $x$ ,  $t(0)$  is the two-way zero-offset time, and  $V_{NMO}$  is the NMO velocity. In the enlarged NMO-corrected view (Figure 10B), the primary seafloor reflection events should ideally be aligned horizontally after correction using the appropriate velocity. In contrast, the OPS, originating from offline sources with different travel paths, does not align horizontally, which helps in its visual discrimination. The red line overlaid on the gathers in Figure 10B indicates the horizon picked by the NN, targeting the true seafloor reflection. Determining the correct mute time manually is challenging due to the interfering OPS and variations in seafloor topography along the survey line. After applying the mute based on the NN picks (Figure 10C), the OPS is mostly removed. However, some residual noise remains, and potential over-muting (clipping the start of the seafloor reflection) is observed in some areas, reflecting the challenges of picking accurately in this domain.

Figure 11A shows sample common receiver gathers where the OPS is visible ahead of the true seafloor reflection. Because these gathers exhibit less moveout delay for the seafloor event compared to shot gathers, NMO correction was not applied before picking. The red line in Figure 11B shows the NN pick for the true seafloor. The resulting mute (Figure 11C) effectively removes the OPS, allowing the true seafloor reflection to be observed more clearly and continuously. The effectiveness in this domain benefits from the relatively long streamer configuration used in the survey, which provides sufficient data redundancy for the NN to learn the patterns.

Finally, for the CDP-offset gathers, OPS can be observed before the stacking result (Figure 12A). After NMO correction, both the OPS and the true seafloor reflection appear relatively flat because their travel paths

are mostly through the water column. The NN pick (red line in Figure 12B) targets the later-arriving true seafloor event. Applying the mute based on these picks removes the OPS (Figure 12C). However, similar to the common shot results, some inaccuracies lead to residual noise or over-muting, especially at the far offset traces. While velocity analysis is typically performed in the CDP-offset domain, which could make OPS removal here convenient, the large number of traces and potential smearing effects during sorting may have made the NN training and picking less consistent compared to the common receiver domain for this dataset.

### 3.2. Quantitative comparison of picking consistency

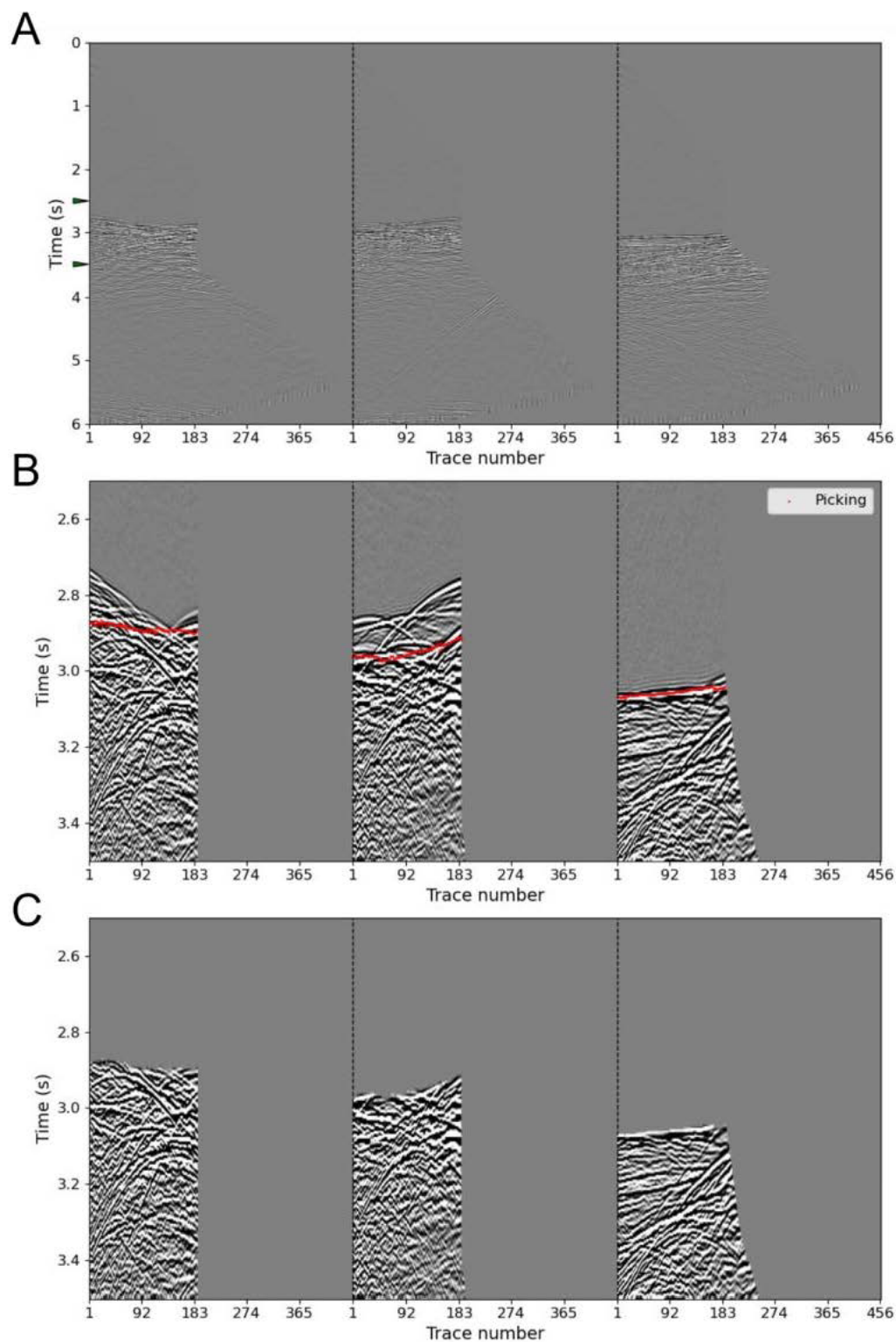
Before stacking the data, we performed a statistical analysis of the NN-picked travel times to quantitatively assess the consistency of the results from each domain (Table 4). The analysis indicates that picking in the common receiver gather domain yielded the most consistent results, as evidenced by the lower standard deviation (67.5 ms) compared to common shot (129.7 ms), and CDP-offset gathers (98.4 ms). This suggests that the cascade-correlation neural network's ability to generalize the trend of the true seafloor reflection was most effective in the common receiver domain, likely due to the more consistent presentation of both the true seafloor event and the OPS pattern in this domain for this dataset.

### 3.3. Analysis of stacked and migrated sections

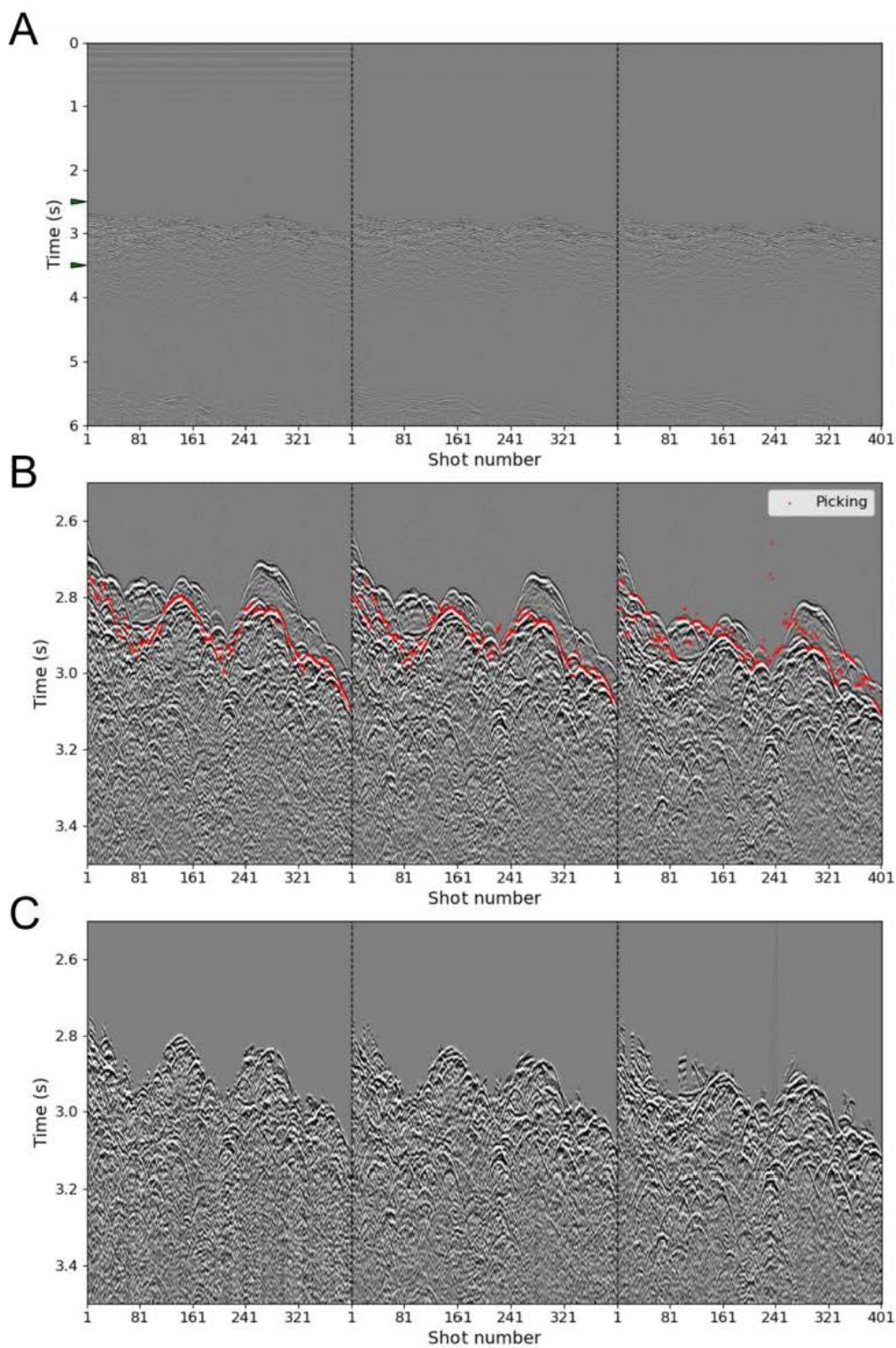
Before analyzing the final stacked sections, the consistency of the picks from the three domains was visually inspected. The picks were transferred and plotted onto a single NMO-corrected CDP gather (CDP 1,401) to directly compare their alignment and flatness, as shown in Figure 13. Note that the lateral coverage of the picks in Figure 13A–C may vary slightly, as the original picking was performed in domains (shot, receiver, and CDP) encompassing different sets of traces relative to CDP 1,401. This comparison provides a visual basis for the quality of the subsequent stacks.

Figure 14 compares the stacked sections after applying the NN pick mute derived from the different gather domains. Muting based on common shot gather picks removed much of the OPS between 2,600 and 3,000 ms, but some residual energy and discontinuities remain along the seafloor reflector, likely due to inconsistencies in the picks from this domain (Figure 14A). Beneath the seafloor event, numerous diffraction hyperbolas are visible, likely originating from irregular subsurface geological structures. On the other hand, muting based on common receiver gather picks yielded the most consistent result (Figure 14B). The quality of the mute appears more consistent,





**Figure 10.** Out-of-plane signal removal workflow in the normal moveout-corrected common shot gather domain at three locations (near common depth points 1,001, 1,301, 1,601). (A) Gathers before muting, showing out-of-plane signal. (B) Neural network pick (red line) targeting the true seafloor reflection. (C) Gathers after applying the neural network-derived mute.



**Figure 11.** Out-of-plane signal removal workflow in the common receiver gather domain at three locations (near common depth points 1,001, 1,301, 1,601). (A) Gathers before muting, showing out-of-plane signal. (B) Neural network pick (red line) targeting the true seafloor reflection. (C) Gathers after applying the neural network-derived mute.

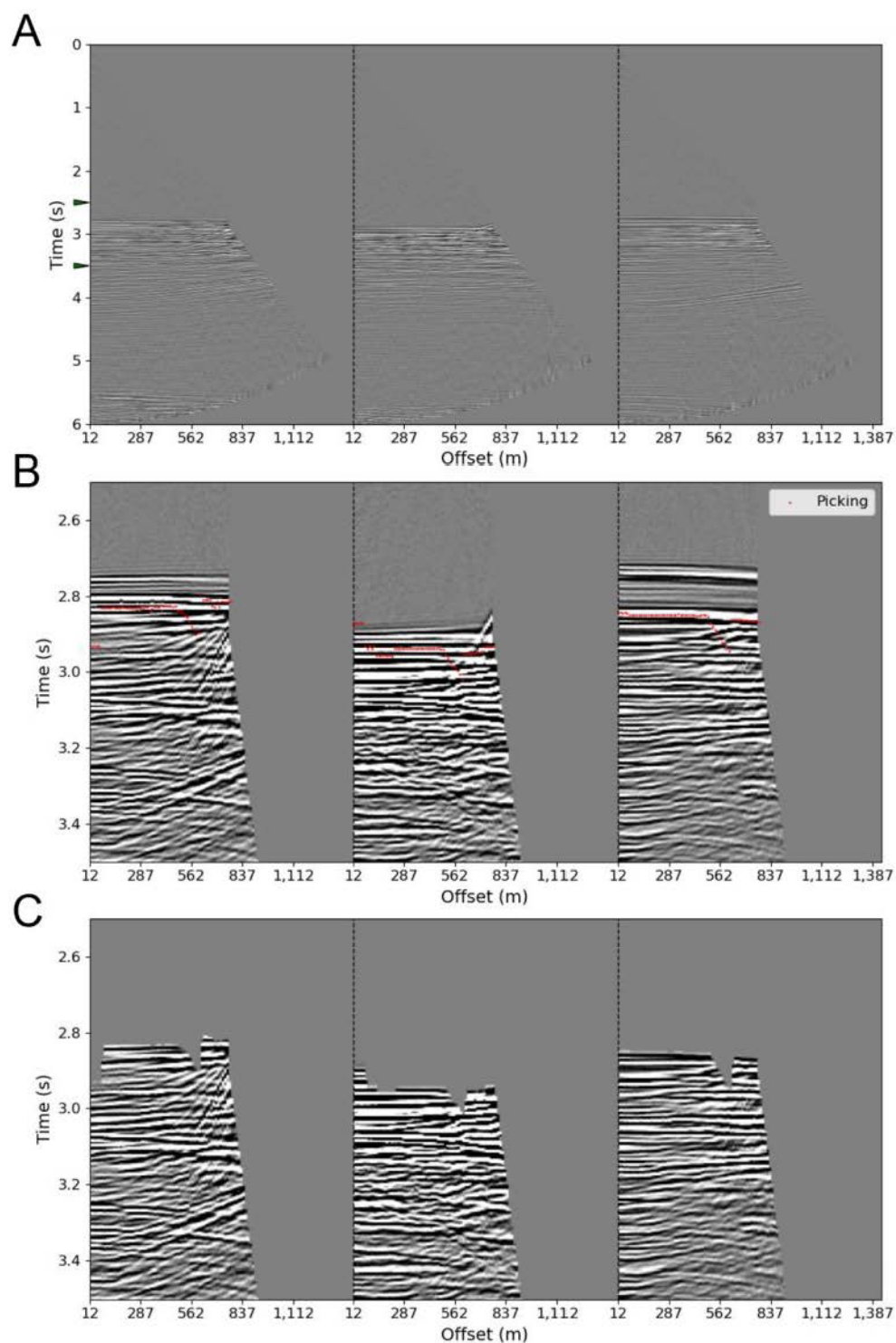


**Figure 12.** Out-of-plane signal removal workflow in the normal moveout-corrected common depth point–offset gather domain at three locations (near common depth points 1,001, 1,301, 1,601). (A) Gathers before muting, showing out-of-plane signal. (B) Neural network pick (red line) targeting the true seafloor reflection. (C) Gathers after applying the neural network-derived mute.

Table 4. Statistics of neural network picking results

Statistic	Common shot gather pick	Common receiver gather pick	Common depth point–offset gather pick
Minimum time	2,518.9	2,688.6	2,534.3
Maximum time	3,206.2	3,108.8	3,131.4
Mean	2,964.2	3,043.6	2,828.7
Standard deviation	129.7	67.5	98.4

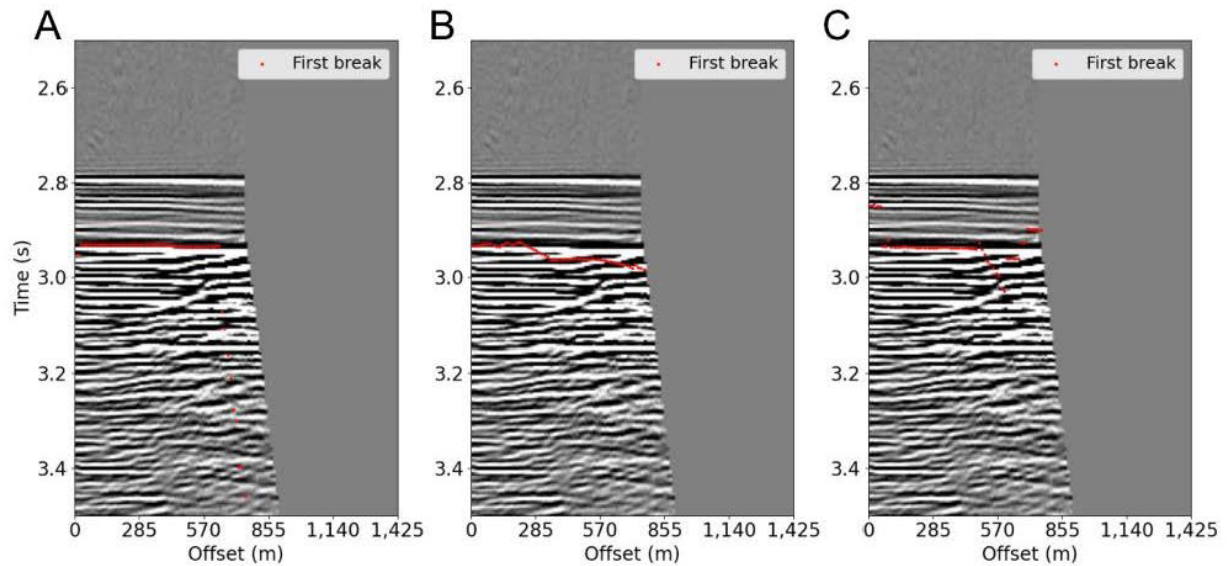


**Figure 13.** Comparison of neural network picking from the three domains, plotted on the normal moveout–corrected common depth point (CDP) gather at CDP 1,401. The picks were derived from the (A) common shot, (B) common receiver, and (C) CDP–offset domains.

resulting in improved continuity of the seafloor event compared to the other domains. Muting based on CDP–offset gather picks showed partial removal of OPS, but the result is similar to the common shot case, with some remaining discontinuities (Figure 14C). The challenges in training the NN effectively in this domain, possibly due to the large number of traces and sorting effects, likely contributed to a less effective outcome.

To collapse diffractions and accurately position the reflections, we applied Kirchhoff post-stack time migration to the muted datasets (Figure 15). This process sums

seismic amplitudes along diffraction curves defined by the migration velocity ( $V_{mig}$ ). The basic principle can be represented by the Kirchhoff summation or integral:<sup>34,35</sup>

$$P_{mig}(x_{out}, t_{out}) \approx \sum_{x_{in}} \omega(x_{in}, x_{out}, t_{out}) P_{stack}(x_{in}, t_{in}(x_{in}, x_{out}, t_{out})) \quad (6)$$

where  $P_{mig}(x_{out}, t_{out})$  is the migrated amplitude at the output location  $x_{out}$  and zero-offset time  $t_{out}$ ,  $P_{stack}(x_{in}, t_{in})$  is the stacked amplitude at the input location  $x_{in}$  and input

time  $t_{in} = \sqrt{t_{out}^2 + \frac{4(x_{in} - x_{out})^2}{V_{mig}^2}}$  (which lies on the diffraction



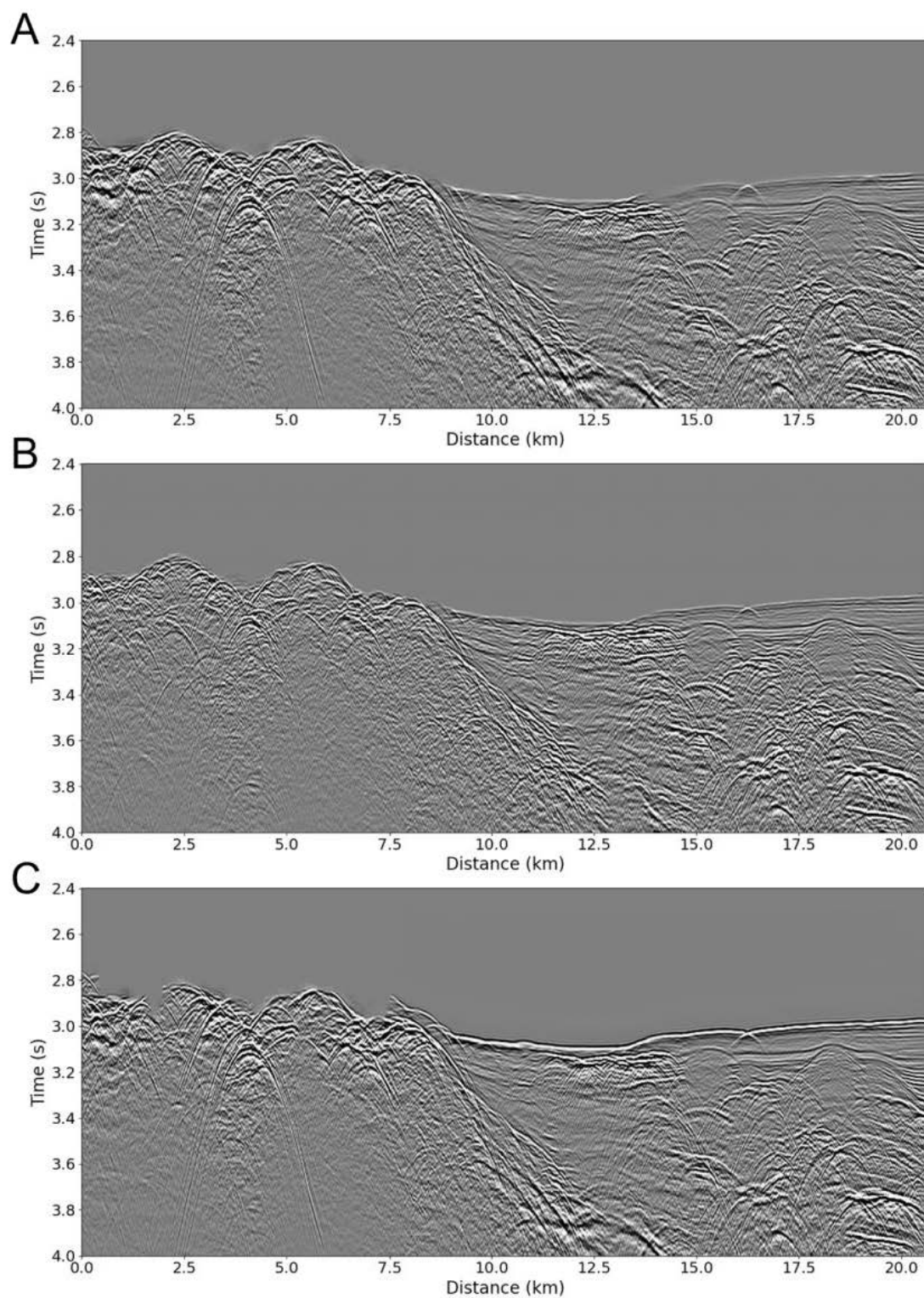


**Figure 14.** Stacked sections after applying the neural network-derived mute in three different domains. (A) Muting in the common shot domain. (B) Muting in the common receiver domain shows the most continuous seafloor reflection. (C) Muting in the common depth point–offset domain.



curve), and  $\omega$  represents appropriate weighting factors (e.g., for amplitude scaling and filtering). Migration improved the image of the seafloor in all cases compared to the stacks. The migrated sections show the correction of diffraction signals originating from below the seafloor, resulting in improved overall image quality compared to the brute stack section. Consistent with the stacked results, the migration of the common receiver gather muted data (Figure 15B) exhibits a cleaner and more continuous seafloor reflection, appearing smoother than the results from the common shot (Figure 15A) and CDP–offset (Figure 15C) muted data. The common shot (Figure 15A) and CDP–offset result (Figure 15C) show improvement over the stack but still appear slightly less continuous than the common receiver result. However, where the OPS and true seafloor reflection overlap significantly in time, full recovery of the primary reflection remains difficult even after muting, as the muting process removes energy but cannot restore the signal masked by the overlap.

### 3.4. Validation against external data

To move beyond qualitative inspection, we quantitatively validated the seafloor picking results using an independent bathymetric reference from the Korea Hydrographic and Oceanographic Agency (KHOA).<sup>20</sup> The KHOA bathymetric profile along the survey line was converted to two-way travel time using a water velocity of 1,480 m/s and compared with the seismic seafloor picks. We defined a travel time-delay metric to evaluate accuracy, computing both the mean absolute error (MAE) and the standard deviation of the time difference at each CDP location. Figure 16 illustrates the metric, where Figure 16A shows the brute stack (identical to the original Figure 4A) with the KHOA seafloor profile (solid line) and, for context, the seafloor inferred from first-arrival reflection (dashed line). Figure 16B shows the header-muted stack (Figure 4B) with the same overlays.

The results, summarized in Table 5, show improvement after applying NN-based OPS suppression. The unprocessed brute stack exhibited an MAE of about 115 ms with a standard deviation of ~33 ms, indicating large discrepancies relative to the true seafloor. A header mute reduced the MAE to ~71 ms, though variability remained high (standard deviation ~41 ms). By contrast, the NN-based workflow achieved lower errors where the stacked sections showed MAE values of approximately 45–61 ms, with reduced variability, and the migrated sections further improved to 47–50 ms MAE with standard deviations generally below 38 ms. In contrast, the F–K filtered stacks retained large errors (MAE ~120–216 ms), nearly as high as or worse than the brute stack, confirming that OPS energy remained and biased the seafloor picks.

Assuming a water velocity of 1,480 m/s, an MAE of 10 ms in two-way travel time corresponds to a depth discrepancy of approximately 7.4 m. Consequently, the reduction in error achieved by the proposed method significantly improves the accuracy of seafloor depth estimation compared to the brute stack. These quantitative metrics demonstrate that NN-aided muting yields a seafloor horizon substantially more consistent with the independent bathymetric reference than either no OPS removal or conventional filtering approaches.

We also compared the seismic images directly with the external reference. Figure 17 overlays the KHOA bathymetry (cyan line) on the brute stack, the header-muted stack, and the final migrated sections. In the brute stack (Figure 17A), strong OPS obscures the true seafloor, resulting in large deviations between the cyan line and the interpreted horizon. With a header mute (Figure 17B), some OPS is attenuated, but the remaining residuals still distort the seafloor pick. In contrast, after applying the NN-based suppression, the final migrated sections (Figure 17C–E) show the reflector aligning much more closely with the true seafloor profile, with notably improved positional consistency in the 2.7–3.0 s window.

Finally, to verify that the coherent energy removed by the workflow corresponds to the OPS noise (and not a legitimate signal), we computed difference sections. Figure 18 shows the absolute difference between the brute stack (Figure 4A) and each final muted stack (Figure 14A–C), focused on a time window of 2.4–3.2 s and the first 8 km of the line. This process highlights the energy eliminated by the mute. The difference displays reveal banded coherent events where the OPS was present, indicating that those events were removed. Notably, in the 2.7–3.1 s range, the shape and location of the removed energy match the OPS noise seen in the original data. Some areas show very little difference (meaning the seafloor event was preserved), whereas areas of intense difference correspond exactly to where OPS interfered. This confirms that the technique targeted and removed the intended OPS signals. It is also worth noting that the CDP–offset gather case shows relatively weaker OPS suppression near 7.5–8 km, where the difference is less pronounced. In contrast, the shot and offset gather domains exhibit clearer energy removal in the same region. This suggests that the effectiveness of the technique can vary by data domain, with shot and offset gathers providing more effective suppression in this dataset.

## 4. Discussion

Seismic data acquired in areas of irregular seafloor morphology often contain OPS that can mask the true

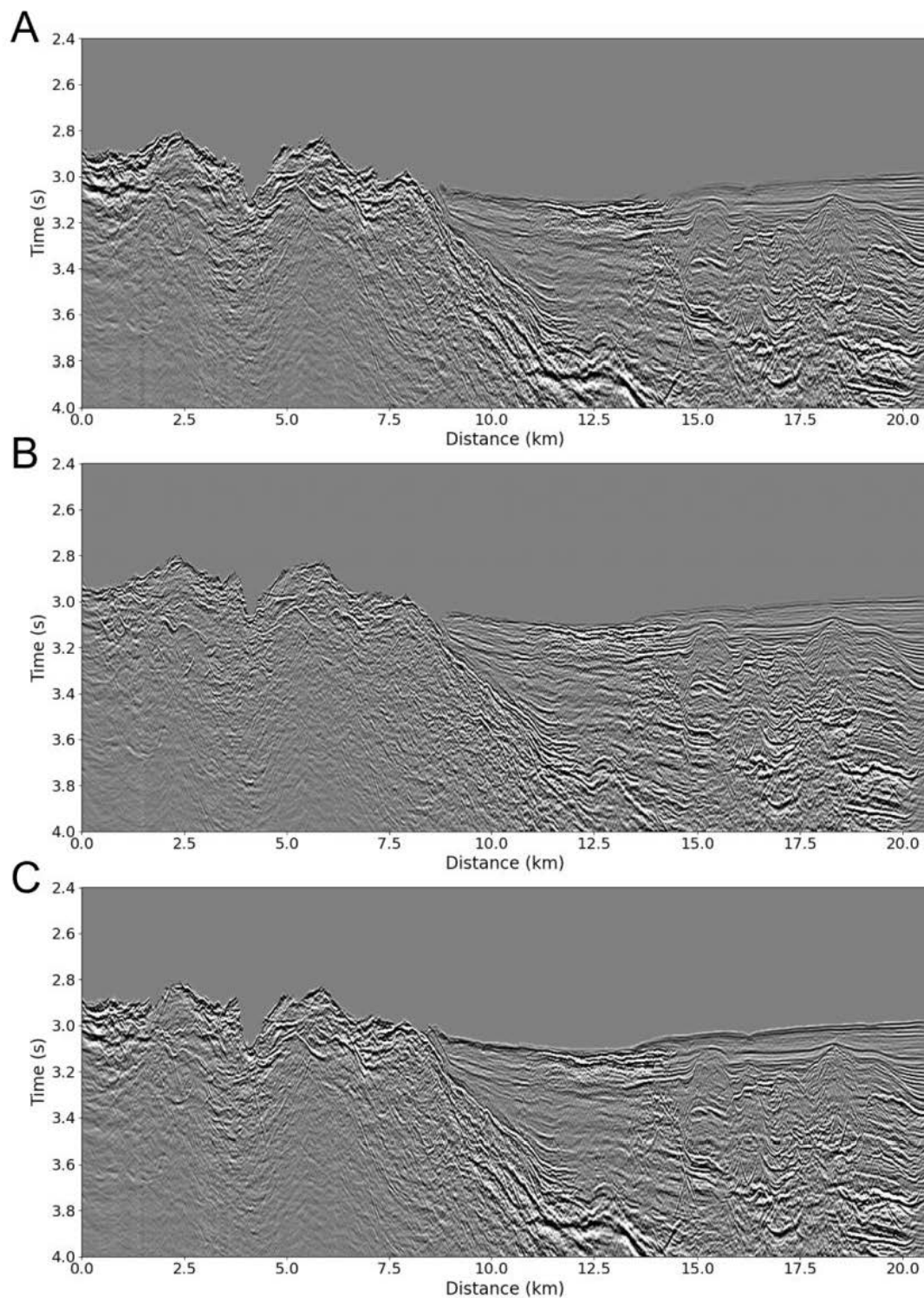


**Figure 15.** Kirchhoff post-stack time migration of the muted sections from [Figure 14](#). (A) Migration of the common shot muted data. (B) Migration of the common receiver muted data. (C) Migration of the common depth point–offset muted data.



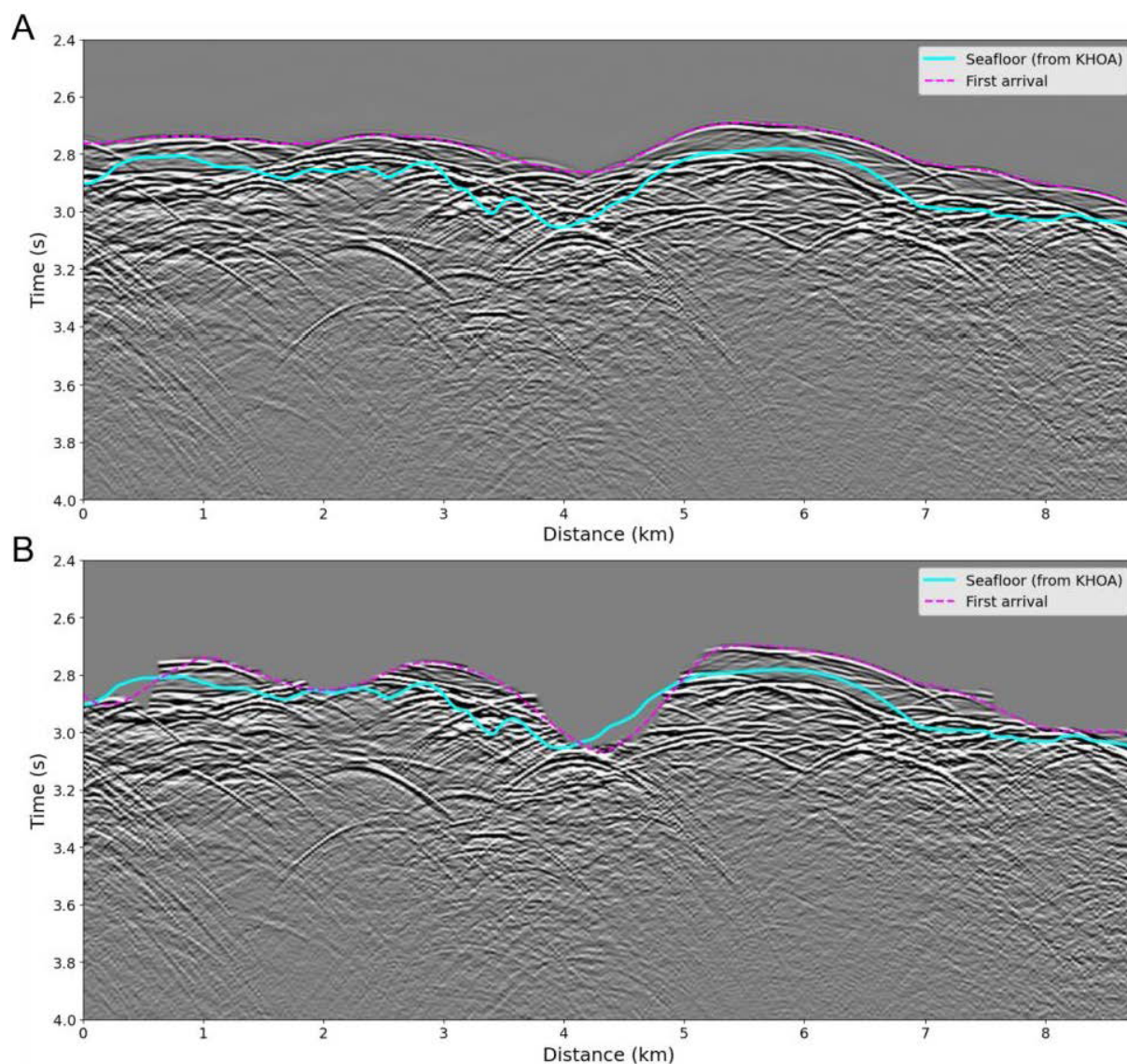


**Figure 16.** Definition of the travel time-delay metric with the external bathymetric reference from the Korea Hydrographic and Oceanographic Agency (KHOA). The KHOA profile (solid line) and the seafloor (dashed line) are overlaid on (A) the brute stack and (B) the header-muted stack.

subsurface image. Identifying and removing these signals is challenging, as they can be coherent and mimic true reflections. Conventional processing techniques, such as simple time gating or frequency-wavenumber filtering, often struggle to effectively isolate and remove OPS without damaging the desired primary reflections, particularly in 2D datasets where the out-of-plane origin cannot be resolved geometrically. As the F-K benchmark in this study demonstrates, the overlap of OPS and the seafloor reflection renders purely dip-based separation ineffective. Simple muting based on header information, like the

water bottom time, was ineffective in this case because the recorded time was itself contaminated by the strong OPS arrivals.

To address this, we sought a method to accurately define a mute function that follows the true seafloor reflection, effectively removing the preceding OPS. We found that NN picking provided a suitable tool for this task. By training the NN on a small set of manually identified true seafloor arrivals within the affected zone, the network learned to recognize and pick this specific event across the dataset, even in the presence of the strong, interfering OPS.

**Table 5. Mean absolute error and standard deviation of the travel time difference between the seismic seafloor pick and an independent bathymetric reference.**

Data	Mean absolute error (ms)	Standard deviation (ms)
Brute stack (Figure 4A)	115.14	32.88
Brute stack after removing out-of-plane signal (OPS) using header mute (Figure 4B)	70.99	41.45
F–K filtered stack section in common shot gather (CSG) (Figure 6A)	120.40	37.28
F–K filtered stack section in common receiver gather (CRG) (Figure 6B)	134.95	41.20
F–K filtered stack section in common depth point (CDP)–offset gather (Figure 6C)	215.53	49.49
Stack section after removing OPS in CSG (Figure 14A)	49.29	33.41
Stack section after removing OPS in CRG (Figure 14B)	45.37	27.09
Stack section after removing OPS in CDP–offset gather (Figure 14C)	61.24	35.87
Migrated section after removing OPS in CSG (Figure 15A)	47.33	26.83
Migrated section after removing OPS in CRG (Figure 15B)	50.37	37.64
Migrated section after removing OPS in CDP–offset gather (Figure 15C)	48.31	30.86

Notes: Results are shown for the brute stack, header-muted stack, the neural network-muted stacks, and migrated sections from the three domains, and the F–K filtered stacks. Lower values indicate better agreement with the reference.

The NN picking approach offers several advantages for this type of targeted noise removal. It is adaptive, learning the specific characteristics of the target event directly from the data. It proved effective even with minimal training data, avoiding the need for large, pre-labeled datasets often required by more complex machine learning models. This study demonstrated the successful application of a technique commonly used for first-arrival picking in land seismic surveys to a different challenge in marine seismic data. While many automated picking algorithms focus solely on first breaks, the NN picker used here could be trained to target a specific later arrival (the true seafloor) based on user guidance. This adaptability makes it a flexible tool for addressing specific noise problems where a particular event needs to be identified and isolated.

While 3D seismic acquisition inherently handles

OPS more effectively by resolving the wavefield in three dimensions, this is often not feasible due to cost constraints, especially when working with legacy 2D data. For such 2D datasets, particularly those acquired with an adequate number of channels (longer streamers provide better pattern definition), the NN picking method offers a practical and effective way to mitigate OPS. The results suggest that the quality of OPS removal improves with better data redundancy.

The ability to produce a clearer image of the true seafloor has significant practical implications. Accurate seafloor imaging is essential for various applications, including geohazard assessment, planning routes for submarine cables or pipelines, and selecting sites for ocean bottom instrumentation. By removing masking OPS, this technique can improve the reliability of interpretations

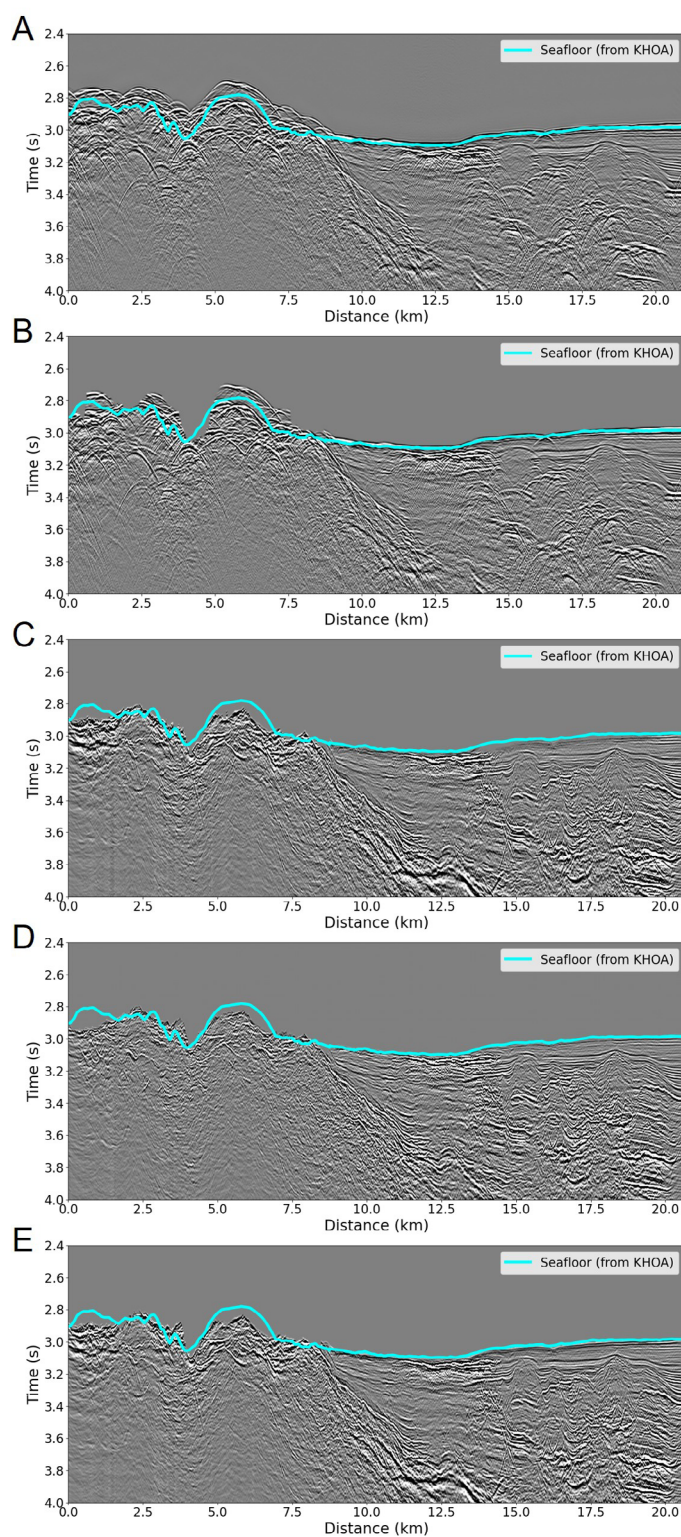


**Figure 17.** Validation by overlaying the Korea Hydrographic and Oceanographic Agency (KHOA) bathymetry profile (cyan line) on seismic sections. (A) The brute stack shows a poor match due to out-of-plane signals. (B) The header-muted stack shows some improvement, but the residual out-of-plane signal remains. (C–E) The final migrated sections after neural network-muting in the (C) common shot, (D) common receiver, and (E) common depth point–offset domains show a much closer alignment with the KHOA profile.



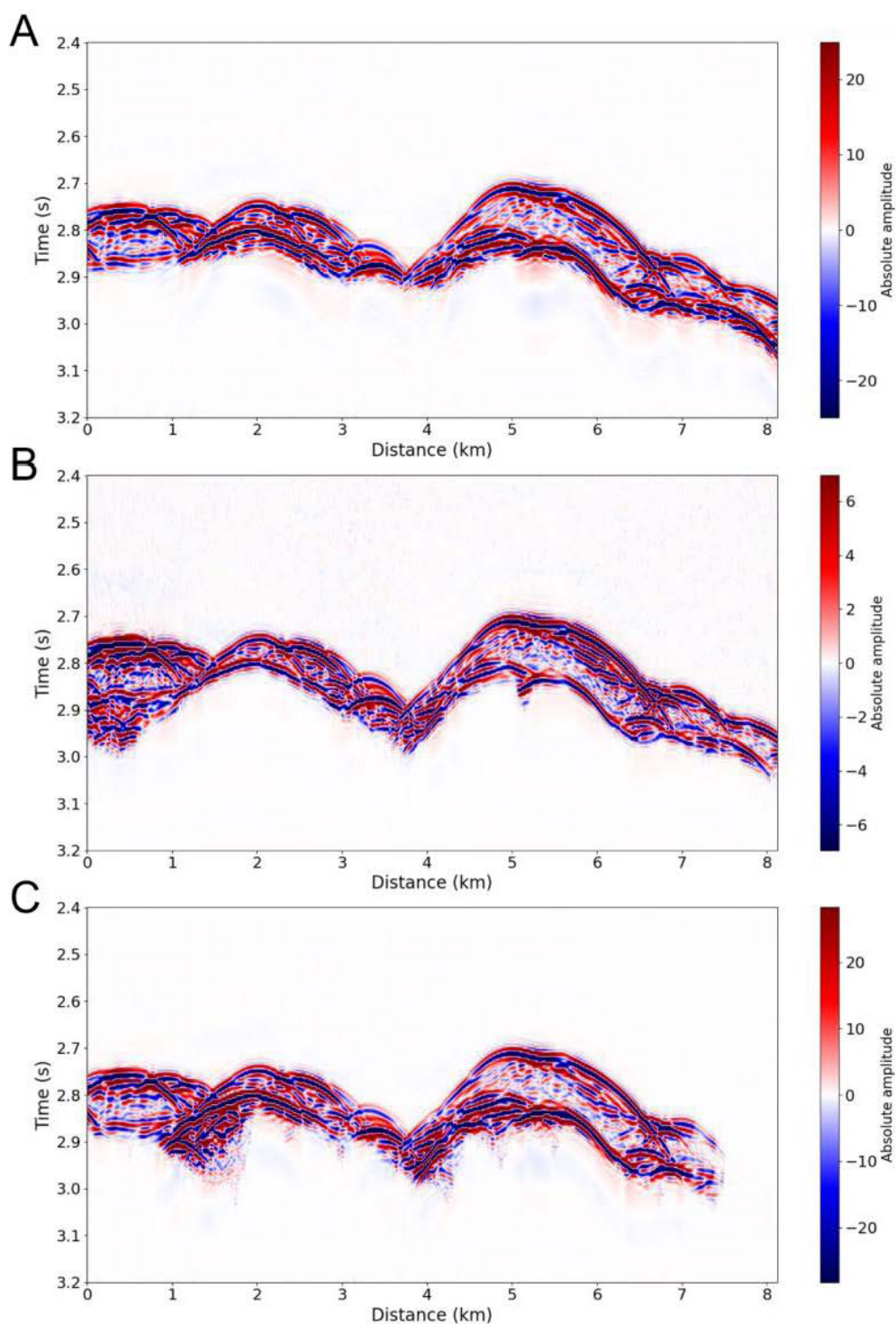


**Figure 18.** Different sections showing the energy removed by the neural network-derived mute. The panels show the absolute difference between the brute stack (Figure 4A) and the muted stacks from the (A) common shot, (B) common receiver, and (C) common depth point–offset domains. The display is limited to 2.4–3.2 s and 0–8 km to emphasize the out-of-plane signal energy targeted by the workflow. The coherent energy corresponds to the removed out-of-plane signal.

based on 2D seismic data for these purposes.

Despite its effectiveness, the proposed method has limitations that suggest directions for future work. Recent advances in deep learning have introduced strategies such as transfer learning (fine-tuning) and few-shot learning to reduce the dependence on large, fully labeled seismic datasets. For example, fine-tuning a pre-trained convolutional neural network has been shown to substantially reduce manual labeling requirements for first-break picking while maintaining competitive accuracy across real surveys.<sup>36</sup> However, multiple studies emphasize that model performance can be highly sensitive to out-of-distribution (domain-shift) conditions related to acquisition configuration and site-dependent noise characteristics, motivating explicit evaluation of cross-environment transferability.<sup>37</sup> Few-shot approaches have also been proposed to adapt seismic interpretation models to new surveys with minimal annotation, but they explicitly note that subsurface heterogeneity can limit label transferability across locations and require careful adaptation mechanisms.<sup>38</sup>

Despite these advances, applying transfer/few-shot paradigms to OPS suppression in legacy 2D marine data faces a critical domain-gap issue. OPS is often strongly site-specific coherent noise generated by unique local 3D bathymetric/topographic conditions (e.g., irregular seamounts), meaning that models pre-trained on generic datasets may experience negative transfer and fail to reliably separate OPS from true in-plane seafloor reflections. In this context, lightweight, interpreter-in-the-loop approaches that learn directly from a small number of site-specific examples can be preferable when the dominant challenge is a locally unique noise mode rather than a broadly recurring texture class.

The NN picking technique, while effective, is not without other limitations. Its success is highly dependent on the quality of the initial user picks, making it a semi-automated process requiring careful human oversight and quality control. This interpreter-in-the-loop design means the technique is not fully automated. An expert must decide on and pick the horizon on key gathers to guide the network. However, this involvement ensures the picked horizon remains geophysically plausible and consistent. Nevertheless, the workflow provides a valuable capability for removing noise that is difficult to address with conventional filtering, though it still requires user expertise. Careful application and validation are essential to ensure the uniqueness and exactness of the picked horizon and the resulting mute. Furthermore, where the OPS and true seafloor reflection are nearly coincident in time, full recovery of the primary reflection remains a

challenge, as the muting process can result in localized over-muting or residual contamination, which contributes to the remaining discrepancies.

Although this study demonstrated the method on a single line, the workflow relies on a site-specific training strategy. This design allows the network to adapt to various geological environments and acquisition geometries by learning the unique morphological characteristics of the signal and noise in each new survey, provided a small set of representative training picks is supplied.

## 5. Conclusion

Rapid variations in seafloor morphology can generate significant OPS on 2D marine seismic data. Because OPS is not ubiquitous in all datasets, standardized removal workflows are less common compared to those for multiples or ghosts. To separate the OPS from the seafloor reflection signal, we focused on the first break picking function by NN picking. Then we transferred it to muting information of seismic traces. To compare mute performance, we trained three different gather domains. Among the three-gather domain muting, the common receiver gather domain result yielded the most consistent picks and the clearest final image of the true seafloor, and it had better results than conventional F-K filtering. Quantitative validation against the KHOA reference data (bathymetry) supports this conclusion. This demonstrates that OPS muting with NN picking, when applied thoughtfully in the appropriate data domain, can be a powerful and practical tool for improving the quality of legacy 2D seismic data suffering from out-of-plane signal contamination.

This methodology could be incorporated into a dedicated workflow for processing 2D seismic data acquired in areas known for irregular seafloor topography, such as near submarine volcanoes or mid-ocean ridges, where OPS is likely to be problematic. Future work could involve testing more advanced machine learning models for signal discrimination, particularly focusing on separating overlapping OPS and primary reflections. Furthermore, the principle of using NN picking to identify specific target horizons amidst noise could potentially be adapted for discriminating other challenging seismic events, such as identifying specific stratigraphic layers in challenging zones or improving first-break picking when early arrivals are contaminated by non-seismic noise sources. We found this application of OPS muting with NN picking, adapted from its typical use, to be a valuable technique improving seafloor imaging.

## Acknowledgments

None.

## Funding

This research was supported by the Basic Research Projects (GP2025-021 and GP2025-025) of the Korea Institute of Geoscience and Mineral Resources (KIGAM), funded by the Ministry of Science and ICT of the Republic of Korea.

## Conflict of interest

The authors declare that they have no competing interests.

## Author contributions

*Conceptualization:* Ganghoon Lee, Snons Cheong

*Formal analysis:* Ganghoon Lee, Snons Cheong

*Investigation:* Ganghoon Lee, Changyoon Lee, Junseok Kwon, Snons Cheong

*Methodology:* Snons Cheong

*Validation:* Ganghoon Lee, Changyoon Lee, Junseok Kwon, Snons Cheong

*Visualization:* Ganghoon Lee, Changyoon Lee, Snons Cheong

*Writing—original draft:* Ganghoon Lee, Changyoon Lee, Junseok Kwon, Snons Cheong

*Writing—review & editing:* Ganghoon Lee, Snons Cheong

## Availability of data

Data associated with this research requires permission from the Korea Institute of Geoscience and Mineral Resources (KIGAM) and can be obtained by contacting the corresponding author.

## References

1. Sheriff RE, Geldart LP. *Exploration Seismology*. Cambridge University Press; 1995.
2. Yilmaz Ö. *Seismic Data Analysis: Processing, Inversion, and Interpretation of Seismic Data*. Society of Exploration Geophysicists; 2001.  
doi: 10.1190/1.9781560801580
3. Drummond BJ, Hobbs RW, Goleby BR. The effects of out-of-plane seismic energy on reflections in crustal-scale 2D seismic sections. *Tectonophysics*. 2004;388(1-4):213-224.  
doi: 10.1016/j.tecto.2004.07.040
4. Larner K, Chambers R, Yang M, Lynn W, Wai W. Coherent noise in marine seismic data. *Geophysics*. 1983;48(7):854-886.  
doi: 10.1190/1.1441516
5. Hobbs RW, Drummond BJ, Goleby BR. The effects of three-dimensional structure on two-dimensional images of crustal seismic sections and on the interpretation of shear zone morphology. *Geophys J Int*. 2006;164(3):490-500.  
doi: 10.1111/j.1365-246x.2006.02814.x
6. Günther RH, Klemperer SL, Goodliffe AM. Modeling sideswipe in 2D oceanic seismic surveys from sonar data: Application to the Mariana arc. *Tectonophysics*. 2006;420(1-2):333-343.  
doi: 10.1016/j.tecto.2006.01.027
7. Tucker PM. *Pitfalls Revisited*. Society of Exploration Geophysicists; 1982.  
doi: 10.1190/1.9781560802341
8. Nedimović MR, West GF. Crooked-line 2D seismic reflection imaging in crystalline terrains: Part 1, data processing. *Geophysics*. 2003;68(1):274-285.  
doi: 10.1190/1.1543213
9. Nedimović MR, West GF. Crooked-line 2D seismic reflection imaging in crystalline terrains: Part 2, migration. *Geophysics*. 2003;68(1):286-296.  
doi: 10.1190/1.1543214
10. U.S. Energy Information Administration. Definitions, sources, and explanatory notes. Independent Statistics and Analysis. Available from: [https://www.eia.gov/dnav/ng/TblDefs/ng\\_enr\\_seis\\_tbldef2.asp](https://www.eia.gov/dnav/ng/TblDefs/ng_enr_seis_tbldef2.asp) [Last accessed on 2025 Nov 20].
11. Biondi BL. *3D Seismic Imaging*. Society of Exploration Geophysicists; 2006.  
doi: 10.1190/1.9781560801689
12. Vermeer GJO. *3D Seismic Survey Design*. 2nd ed. Society of Exploration Geophysicists; 2012.  
doi: 10.1190/1.9781560803041
13. Micenko M. Seismic window: Pitfalls revisited. *Preview*. 2019;2019(200):40.  
doi: 10.1080/14432471.2019.1621248
14. Stewart RR, Marchisio G. Side-scanning seismic: Analysis and a physical modeling study. In: *SEG Technical Program Expanded Abstracts 1991*. 61st SEG Annual International Meeting; November 10-14, 1991; Houston, TX. Society of Exploration Geophysicists; 1991:679-682.  
doi: 10.1190/1.1889180
15. Duren RE, Morris SV. Sideswipe removal via null steering. *Geophysics*. 1992;57(12):1623-1632.  
doi: 10.1190/1.1443229
16. Beckel RA, Juhlin C. The cross-dip correction as a tool to improve imaging of crooked-line seismic data: a case study from the post-glacial Burträsk fault, Sweden. *Solid Earth*. 2019;10(2):581-598.  
doi: 10.5194/se-10-581-2019
17. Mancuso C, Naghizadeh M. Generalized cross-dip moveout correction of crooked 2D seismic reflection surveys. *Geophysics*. 2021;86(4):V285-V298.

- doi: 10.1190/geo2020-0278.1
18. Alkhalifah TA, Biondi B. Numerical analysis of the azimuth moveout operator for vertically inhomogeneous media. *Geophysics*. 2004;69(2):554-561.  
doi: 10.1190/1.1707075
  19. Khoshnavaz MJ. Oriented time-domain dip moveout correction for planar reflectors in common-source domain. *Geophysics*. 2017;82(6):U87-U97.  
doi: 10.1190/geo2016-0577.1
  20. Korea Hydrographic and Oceanographic Agency. Bathymetric Data (BADA2024). Badanuri Marine Information Service. Available from: <https://www.khoa.go.kr/oceandata/oceaninfo/map.do?lang=en> [Last accessed on 2026 Mar 18].
  21. Lee GH, Kim HJ, Han SJ, Kim DC. Seismic stratigraphy of the deep Ulleung Basin in the East Sea (Japan Sea) back-arc basin. *Mar Pet Geol*. 2001;18(5):615-634.  
doi: 10.1016/s0264-8172(01)00016-2
  22. Ryu BJ, Riedel M. Gas hydrates in the Ulleung Basin, East Sea of Korea. *Terr Atmos Ocean Sci*. 2017;28(6):943-963.  
doi: 10.3319/tao.2017.10.21.01
  23. Murat ME, Rudman AJ. Automated first arrival picking: A neural network approach. *Geophys Prospect*. 1992;40(6):587-604.  
doi: 10.1111/j.1365-2478.1992.tb00543.x
  24. McCormack MD, Zaucha DE, Dushek DW. First-break refraction event picking and seismic data trace editing using neural networks. *Geophysics*. 1993;58(1):67-78.  
doi: 10.1190/1.1443352
  25. Pu Y, Zhang X. Application of deep learning in first break picking of seismic data. In: *Proceedings of the SEG 2018 Workshop: SEG Maximizing Asset Value Through Artificial Intelligence and Machine Learning*. SEG 2018 Workshop; September 17-19, 2018; Beijing, China. Society of Exploration Geophysicists and Chinese Geophysical Society; 2018:19-21.  
doi: 10.1190/aiml2018-05.1
  26. Tsai KC, Hu W, Wu X, Chen J, Han Z. Automatic first arrival picking via deep learning with human interactive learning. *IEEE Trans Geosci Remote Sens*. 2020;58(2):1380-1391.  
doi: 10.1109/tgrs.2019.2946118
  27. Bornstein T, Lange D, Münchmeyer J, et al. PickBlue: Seismic phase picking for ocean bottom seismometers with deep learning. *Earth Space Sci*. 2023;11(1):e2023EA003332.  
doi: 10.1029/2023ea003332
  28. Niksejel A, Zhang M. OBSTransformer: a deep-learning seismic phase picker for OBS data using automated labelling and transfer learning. *Geophys J Int*. 2024;237(1):485-505.  
doi: 10.1093/gji/ggae049
  29. Pham N, Li W. Physics-constrained deep learning for ground roll attenuation. *Geophysics*. 2021;87(1):V15-V27.  
doi: 10.1190/geo2020-0691.1
  30. Cui Y, Wu J, Bai M, Chen Y. Ground-truth-free deep learning for 3D seismic denoising and reconstruction with channel attention mechanism. *Geophysics*. 2024;89(6):V503-V520.  
doi: 10.1190/geo2023-0592.1
  31. Fu X, Cao D, Zhang F. Deep-learning-based denoising of prestack seismic angle gathers with application to time-lapse data. *Geophysics*. 2025;91(1):WA11-WA21.  
doi: 10.1190/geo2024-0472.1
  32. Fahlman SE, Lebiere C. The cascade-correlation learning architecture. In: Touretzky D, ed. *Advances in Neural Information Processing Systems 2*. NIPS'89: Neural Information Processing Systems; November 27-30, 1989; Denver, CO. MIT Press; 1990:524-532.
  33. Li Z, Sheng R, Xu W, Yang J. The improvement of neural network cascade-correlation algorithm and its application in picking seismic first break. *Adv Pet Explor Dev*. 2013;5(2):41-51.  
doi: 10.3968/j.aped.1925543820130502.1503
  34. Schneider WA. Integral formulation for migration in two and three dimensions. *Geophysics*. 1978;43(1):49-76.  
doi: 10.1190/1.1440828
  35. Bleistein N. On the imaging of reflectors in the Earth. *Geophysics*. 1987;52(7):931-942.  
doi: 10.1190/1.1442363
  36. Mardan A, Blouin M, Fabien-Ouellet G, Giroux B, Vergniault C, Gendreau J. A fine-tuning workflow for automatic first-break picking with deep learning. *Near Surf Geophys*. 2024;22(5):539-552.  
doi: 10.1002/nsg.12316
  37. St-Charles PL, Rousseau B, Ghosn J, Bellefleur G, Schetselaar E. A deep learning benchmark for first break detection from hardrock seismic reflection data. *Geophysics*. 2023;89(1):WA279-WA294.  
doi: 10.1190/geo2022-0741.1
  38. Papadopoulos T, Mosser L, Oikonomou D, Naeini EZ, Karantzas K. Few-shot Learning for Semantic Segmentation of Seismic Data. In: *82nd EAGE Annual Conference & Exhibition*. 82nd EAGE Annual Conference & Exhibition; October 18-21, 2021; Amsterdam, Netherlands. European Association of Geoscientists & Engineers; 2021:1-5.  
doi: 10.3997/2214-4609.202113255